Sara Isabel Rodrigues Inocêncio

Licenciada em Ciência de Engenharia Química e Bioquímica

Chemical-physical study of ibuprofen incorporated into unmodified and modified mesoporous silicas: from matrix synthesis to drug release

Dissertação para do Grau de Mestre em
Engenharia Química e Bioquímica

Orientador: Teresa Cordeiro, Aluna de doutoramento, FCT-UNL

Co-orientadores: Marta Corvo, Pós-Doc, FCT-UNL
Madalena Dionísio Andrade, Professora Auxiliar, FCT-UNL

Júri:

Presidente: Professor Doutor Mário Fernando José Eusébio

Arguente: Doutora Teresa Maria Alves Casimiro Ribeiro

FACULDADE DE CIÊNCIAS E TECNOLOGIA
UNIVERSIDADE NOVA DE LISBOA

Setembro 2018

Sara Isabel Rodrigues Inocêncio

Licenciada em Ciências de Engenharia Química e Bioquímica

Chemical-physical study of ibuprofen incorporated into unmodified and modified mesoporous silicas: from matrix synthesis to drug release

Dissertação para obtenção do Grau de Mestre em

Engenharia Química e Bioquímica

Orientador: Teresa Cordeiro, Aluna de doutoramento, FCT-UNL

Co-orientadores: Marta Corvo, Pós-Doc, FCT-UNL
Madalena Dionísio Andrade, Professora Auxiliar, FCT-UNL

Júri:

Presidente: Professor Doutor Mário Fernando José Eusébio

Arguentes: Doutora Teresa Maria Alves Casimiro Ribeiro

Setembro 2018

Chemical-physical study of ibuprofen incorporated into unmodified and modified mesoporous silicas: from matrix synthesis to drug release

Agradecimentos

Finda esta etapa tão importante do meu percurso académico, não posso deixar de agradecer a todos aqueles que, de alguma forma, me acompanharam, incentivaram e contribuíram decisivamente para o sucesso desta “viagem”.

Como não poderia deixar de ser, as minhas primeiras palavras são para a minha co-orientadora, a Professora Doutora Madalena Dionísio, de uma disponibilidade inexcedível, e que desde o primeiro momento me acolheu no seu laboratório, proporcionando-me diversas oportunidades para melhorar as minhas capacidades, ajudando-me a desenvolver os meus conhecimentos e a crescer profissionalmente.

À futura Doutora Teresa Cordeiro, pela enorme disponibilidade e pelo apoio em todos os momentos, tanto ao nível científico como emocional, sempre com uma palavra de encorajamento e de força.

À Professora Doutora Marta Corvo por me ter orientado na aquisição de conhecimentos numa área que, até então, me era totalmente desconhecida, RMN de sólidos.

À investigadora Inês Matos pelo acompanhamento em laboratório, na síntese das sílicas, e pelo apoio ao longo de todo o processo de elaboração deste trabalho.

À Universidade Lille 1 – Ciências e Tecnologias, em França, pelas análises realizadas que em muito contribuíram para o desenvolvimento do meu estudo.

Ao Professor Doutor João Sotomayor pelo auxílio com as amostras preparadas em atmosfera sob vácuo.

A todos do Laboratório 122 com quem tive o prazer de conviver, em especial à Piedade D’Orey e à Andreia Santos, pelo companheirismo, pela amizade, pelo apoio e pela transmissão de conhecimentos. Recordar-vos-ei sempre como pessoas especiais que foram nesta fase importante da minha vida.

Por fim, agradeço aos meus Pais e restante Família por todo o carinho, pela paciência e pelas palavras de incentivo com que sempre me presentearam. A eles, dedico este trabalho.

Resumo

Este trabalho visa racionalizar o perfil de libertação de um fármaco pouco solúvel em água impregnado em matrizes de sílica mesoporosas, através das interações hóspede-hospedeiro. A incorporação de fármacos em matrizes é amplamente utilizada como estratégia para estabilizar o estado amorfo e simultaneamente aumentar a solubilidade dos fármacos atualmente comercializados. O ibuprofeno (Ibu) que contém propriedades antipiréticas, analgésicas e anti-inflamatórias, foi impregnado em duas sílicas inorgânicas mesoporosas MCM-41, com e sem modificação por sililação (MCM-41$_{sil}$). A análise de porosimetria de azoto exibiu uma estreita distribuição de tamanho de poro, característica deste tipo de sílica. O sucesso da modificação da superfície da sílica foi confirmado por espectroscopia de infravermelho (ATR-FTIR), ressonância magnética nuclear em estado sólido (ssNMR) e análise de porosimetria de azoto.

A impregnação do fármaco foi realizada por capilaridade sob vácuo e os compósitos resultantes analisados por espectroscopia termogravimetria (TGA), calorimetria diferencial de varrimento (DSC), ATR-FTIR e ssNMR. A presença de uma transição vítrea característica da amorfização do Ibu, deslocada para temperaturas mais altas, e a ausência do pico de fusão (T_m = 77 ℃) por DSC juntamente com os dados de TGA que evidenciam um perfil de decomposição em duas etapas, vem confirmar a presença de duas populações moleculares diferentes, uma semelhante ao ibuprofeno nativo e outra a interatuar com as paredes dos poros. Este efeito é mais evidente no ibuprofeno impregnado em MCM-41$_{sil}$ devido a interações mais fortes do hóspede com a superfície do hospedeiro mesoporoso.

Os ensaios de dissolução/libertação do fármaco nos compósitos foram realizados em solução tampão de fosfato, pH 6.8, 37 ℃ e 100 rpm, de modo a simular o fluído intestinal. A quantificação foi efetuada por espectroscopia UV-VIS, a 222 nm e os resultados ajustados utilizando diferentes modelos cinéticos. Ambos os compósitos mostraram ser eficientes como sistemas de libertação do ibuprofeno, apresentando o Ibu impregnado em MCM-41$_{sil}$ uma taxa de libertação do fármaco inferior, o que corrobora os resultados obtidos por DSC e TGA que mostravam uma maior interação do fármaco com a matriz.

Keywords: Ibuprofeno, amorfização, silicas mesoporosas, libertação controlada.

Abstract

This work aims to rationalize the release profile of a poorly water-soluble drug loaded in mesoporous silica matrices, in terms of guest-host interactions. The incorporation of pharmaceutical drugs in a matrix was extensively studied as a strategy to stabilize the amorphous form and simultaneously enhance the solubility of currently commercial drugs. Ibuprofen (Ibu) containing antipyretic, analgesic and anti-inflammatory properties was loaded with two mesoporous inorganic silicas MCM-41, with and without modification by silylation (MCM-41$_{sil}$). Nitrogen adsorption-desorption analysis exhibited a narrow pore size distribution characteristic of this type of silica. The success of the silica surface modification was confirmed by infrared spectroscopy (ATR-FTIR), solid state nuclear magnetic resonance (ssNMR) and nitrogen porosimetry analysis.

The drug loading was performed by capillarity under vacuum and the resulting composites were spectroscopic analyzed by thermogravimetric (TGA), differential scanning calorimetry (DSC), ATR-FTIR and ssNMR. The presence of a glass transition characteristic of ibuprofen amorphization, shifted to higher temperatures, and the absence of the melting peak (T_m = 77 ºC) by DSC together with the TGA data showing a two-step decomposition profile confirm the presence of two different molecular populations, one more bulk-like and another one in a closer interaction with the pore walls. This effect is most evident in ibuprofen loaded in MCM-41$_{sil}$ due to stronger host interactions with the surface of the mesoporous host.

The drug release studies in the composites were performed in phosphate buffer solution, pH 6.8, 37 ℃ and 100 rpm, to simulate the intestinal fluid and analyzed at 222 nm with UV-VIS spectroscopy and the results adjusted using different kinetic models. Both composites were shown to be efficient as ibuprofen release systems, with the ibuprofen loaded in MCM-41$_{sil}$ presented a lower release rate, which corroborates the results obtained by DSC and TGA showing a greater interaction of the drug with the matrix.

Keywords: Ibuprofen, amorphization, mesoporous silicas, drug delivery control.

Index

Figure Index

Table Index

List of Abbreviation

^{13}C NMR	Carbon 13 Nuclear Magnetic Resonance
^{29}Si NMR	Silicon 29 Nuclear Magnetic Resonance
A	Absorbance
$Area_{endo\ transition}$	Area of the melting endothermic transition peak
ATR-FTIR	Attenuated Total Reflectance Fourier Transform Infrared
BCS	Biopharmaceutical Classification System
COX-1	Non-selective cyclooxygenase inhibitor of the enzymes 1
COX-2	Non-selective cyclooxygenase inhibitor of the enzymes 2
CP	Cross Polarization
c_p	Specific heat capacity
CYP2C9	Enzyme cytochrome P450 2C9
DSC	Differential Scanning Calorimetry
H	Enthalpy
Ibu	Ibuprofen
Ibu:MCM-41	Ibuprofen loaded in unmodified MCM-41 silica
Ibu:MCM-41$_{sil}$	Ibuprofen loaded in modified MCM-41 silica
IR	Infrared spectroscopy
m	Mass
MAS	Magic-angle spinning
MCM-41	Mobile Crystalline Material No. 41
MCM-41$_{sil}$	Mobile Crystalline Material No. 41 modified by silylation with mehtyltrimethoxysilane
NSAID	Nonsteroidal anti-inflammatory drug
Q^n	Silicon signal site with four oxygen first neighbors; n corresponding to the number of silicon second neighbors
SBA-15	Santa Barbara Amorphous material No. 15
ssNMR	Solid State Nuclear Magnetic Resonance
T	Transmittance

T_c	Crystalization temperature
T_e	Extrapolated onset melting temperature
TEOS	Tetraethyl orthosilicate
$T_{g,endset}$	Endset glass transition temperature
$T_{g,midpoint}$	Midpoint glass transition temperature
$T_{g,onset}$	Onset glass transition temperature
TGA	Thermogravimetric Analysis
T_m	Melting temperature
T^n	Silicon signal site with three oxygen first neighbors; n corresponding to the number of silicon second neighbors
T_o	Onset melting temperature
UV-VIS	Visible spectroscopy
V	Volume
$\Delta c_p / \Delta t$	Rate of heat capacity change
ΔH_c	Crystallization enthalpy
ΔH_m	Melting enthalpy
$\Delta Q / \Delta t$	Heat flow
$\Delta T / \Delta t$	Rate of heat change

1 Introduction

Currently commercial available drugs, as well as new candidates, have poor solubility in aqueous systems [1]. This difficulty is reduced using excessive dosage, which in addition to causing undesirable side effects to the patient, has a negative impact in the aquatic and terrestrial environment [2,3].

In the pharmaceutical industry, several approaches have been designed to address the delivery challenges presented by poorly soluble drugs. These approaches can be organized into three categories according to the type of alteration involved (Figure 1) [4].

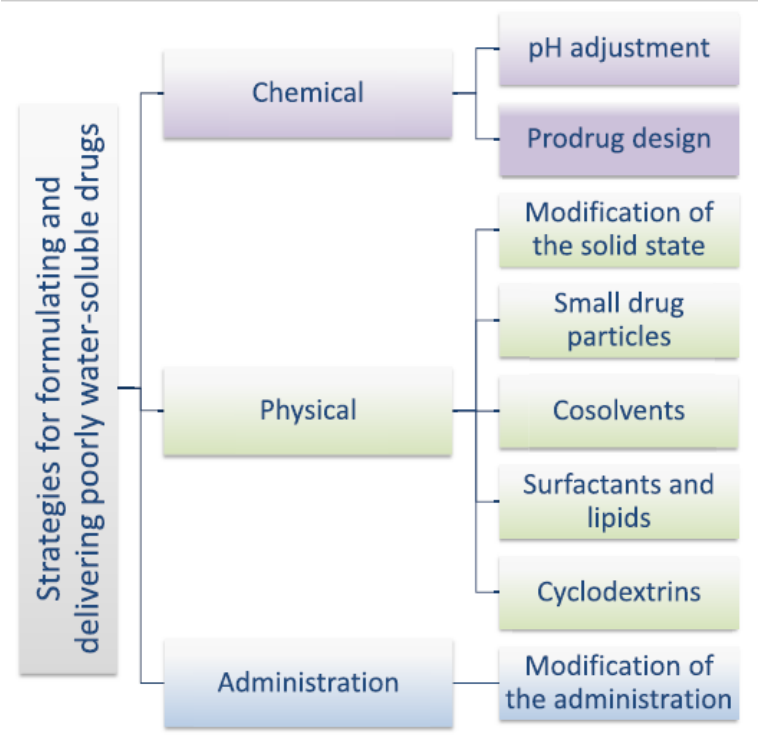

Figure 1 - schematic representation of the different strategies for delivering poorly water-soluble drugs (retrieved from 4).

One option consists in obtaining the pharmaceutical compound in states with higher internal energy, such as amorphous or metastable polymorphisms (modification of the solid state in Figure 1) [5]. Since these states exhibit an intrinsic disorder with respect to their more thermodynamically stable form, the crystalline form, they attain an increase in solubility, and presumably, an increase in bioavailability. Bioavailability is one of main pharmacokinetic properties, which expresses the rate at which the drug is adsorbed, making it available at the target site [6]. However, the amorphous form is thermodynamically unstable, and as such, a strategy is needed to overcome this instability.

In this project, to overcome the instability of the amorphous form, mesoporous silica matrices are used as host structures for the drug. With the tuning of silica pore size and surface

type, it is intended to optimize the amorphization conditions of the drug and study the host-guest (silica-drug) interactions which determine the adsorption and release behaviors of drugs.

1.1 Ibuprofen

Ibuprofen is a nonsteroidal anti-inflammatory drug (NSAID), crystalline at room temperature, indicated for the treatment of pain (analgesic), fever (antipyretic) and inflammation (anti-inflammatory) [7]. Its designation derived from the initials of isobutylpropanoic acid or isobutylphenylpropanoic acid (Figure 2).

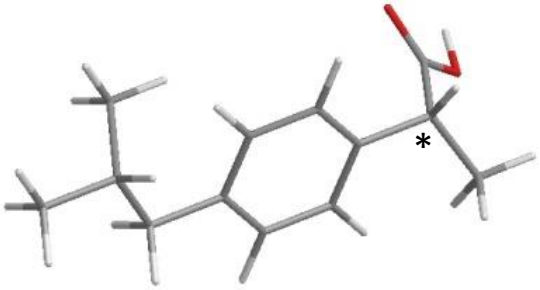

*Figure 2 - 3D chemical structure of Ibuprofen. Grey corresponds to carbon, red to oxygen and white to hydrogen atoms. * Indication of the chiral center.*

In the 60's its synthetic procedure was patented by Boot Pure Drug Company, being marketed under various denominations like Brufen, Advil or Nurofen. It's commercialized in a racemic mixture of S(+)-Ibuprofen and R(-)-Ibuprofen with the enantiomer R being converted *in vivo* into the pharmacologically active form, S(+)-Ibuprofen [8].

Ibuprofen is synthesized by Friedel-Crafts reactions, specifically acylation reactions, using butylbenzene as feedstock. A process has recently been developed by the Hoechst Company, in which catalysts are used to reduce the synthesis steps [9].

The Biopharmaceutical Classification System (BCS) is a regulatory tool introduced in the mid-1990s used to classify the drug substances into four classes (Figure 3) with respect to their aqueous solubility and intestinal membrane permeability [1].

Class	Solubility	Permeability
I	High	High
II	Low	High
III	High	Low
IV	Low	Low

Figure 3 - BCS classification table of a pharmaceutical compound (retrieved from 10).

According to BCS, Ibuprofen was classified as class II drug - substances in which solubility enhancement can improve the oral bioavailability [1,11].

In the body, it binds to the protein albumin and acts as a non-selective cyclooxygenase inhibitor of the enzymes 1 and 2 (COX-1 and COX-2), preventing the formation of pro-inflammatory mediators. Absorption in the gastrointestinal tract is approximately 80%, with a peak plasma concentration within 1.5-2 hours of oral administration. It's metabolized in the liver through oxidation reactions by the enzyme cytochrome P450 2C9 (CYP2C9) and eliminated by renal excretion [12].

1.2 Crystallization

Crystallization results from a combination of two processes, nucleation and crystal growth, being required the presence of a nucleus on which the crystal will subsequently grow.

In nucleation, small groups of molecules assembly together forming clusters that ideally stabilize and make up the nuclei. For this stabilization the clusters need to reach a critical size that depends on factors such as temperature. It's in this process that the molecules organize themselves periodically in a defined crystalline structure [13]. If the nucleation is rapid, the formation of clusters will be almost simultaneous, resulting in crystals of relatively identical dimensions. On the other hand, if the nucleation is slow, new clusters will nucleate at different times resulting in crystals of various sizes [14].

As mentioned before, the growth of crystals is a process dependent on the nucleation since when cooled in the absence of nuclei the material forms a glass. Crystallization occurs at temperatures between T_g and T_m, and the optimal nucleation temperatures doesn't necessarily coincide with the optimal crystal growth temperature, as shown in Figure 4.

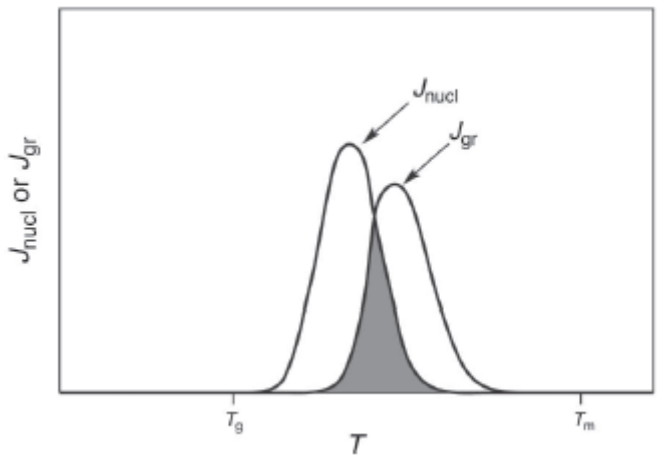

Figure 4 - Representation of the nucleation rate and crystal growth, J_{nucl} and J_{gr} respectively, as a function of temperature (retrieved from 13).

And so, temperature becomes an important factor in crystallization. In the nucleation low temperatures favor thermodynamically this process forming stable clusters, however higher temperatures favor kinetically, due to the decrease of the viscosity. The crystal growth process is favored by the decrease of the temperature below the T_m, although at very low temperatures occurs a reduction in the crystal growth [13].

1.3 Glass transition

The amorphous or vitreous solid is characterized by a disordered molecular structure shared with liquid material, not exhibiting the three-dimensional long-range order of crystalline materials. Thus, the materials on the amorphous state (glasses) have significantly different physical properties of those in the crystalline state. The glass transition occurs when the liquid is cooled below the melting point fast enough to avoid a molecular arrangement and therefore crystallization [15]. This equilibrium deviation happens because the viscosity of the material increases sharply while the temperature decreases, resulting in materials that solidify via a gradual increase in viscosity rather than by crystallization [16].

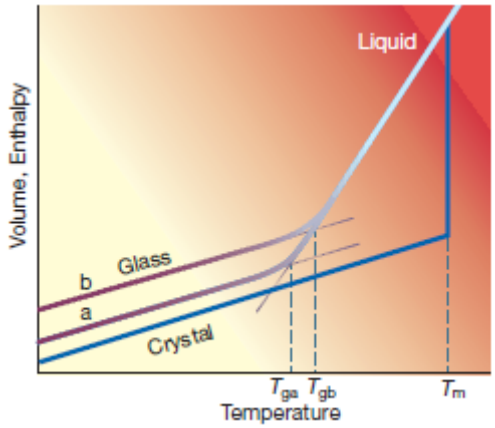

Figure 5 - Phase diagram of a compound with the ability of crystallize and form two types of amorphous materials, where in (a) the cooling rate is less than in (b) (retrieved from 15*).*

Through Figure 5, it's seen that upon cooling below the freezing temperature (T_m), the molecular motion slows down, and consequentially molecules cannot organize in a crystalline configuration in the available time allowed by the cooling rate, consequently the material follows to a supercooled liquid. With subsequent cooling, the volume (V) and enthalpy (H) slope changes at a temperature known as the glass transition temperature (T_g). The slower the cooling rate the longer the time available for configurational arrangement and the colder it can become before falling out of liquid-state equilibrium (Figure 5, glass (a) and (b)). It's verified that in the amorphous state the material possesses better thermodynamic properties in relation to crystalline state, such as higher molecular movement and chemical reactivity. Possessing a spontaneous tendency in

crystallizing below and above the T_g as well, becoming essential the study of strategies to suppress the chemical and physical instability of compounds in the amorphous state [15].

1.4 Mesoporous silica MCM-41

Mobile Crystalline Material No. 41 (MCM-41) became the most popular member of the family of silicate and aluminosilicate mesoporous materials discovered in 1992 by Mobil Oil Corporation, obtained by hydrothermal synthesis and liquid templating mechanism. Such materials exhibit remarkable features such as regular pore system consisting of a hexagonal arrangement of unidimensional, hexagonally shaped pores. These materials possess interesting physical characteristics such as pore diameter control capability in the range of 2 to 10 nm, high surface area up to 1500 $m^2 g^{-1}$, a specific pore volume up to 1.3 mL g^{-1} and excellent thermal, hydrothermal and hydrolytic stabilities. The walls of the pores consist of amorphous SiO_2 with a porosity up to 80% of their total volume. Because of these characteristics it becomes suitable in catalytic applications for various chemical reactions, an adsorbent in wastewater treatment, matrix for controlled release of drugs and model substance for sorption of various gases and vapors [17,18].

For the controlled drug release study, MCM-41 is selected because of the high *in vivo* tolerance of silica currently being used in some pharmaceutical formulations, their size and regular pore system, their relatively easy synthesis and the fact that this mesoporous silica has been proposed as a convenient material for the delivery of drugs [19].

1.5 Mesoporous silica SBA-15

Santa Barbara Amorphous material No. 15 (SBA-15), along with MCM-41, are the most common types of mesoporous matrices. It was discovered by the University of California at Santa Barbara (UCSB) in 1998. Like other mesoporous matrices, the SBA-15 presents a hexagonal pore arrangement as well as all the interesting intrinsic physical characteristics such as stable and uniform mesoporous structures, large surface areas and well-defined surface properties for applications in shape-selective catalysis reactions or separation involving large molecules, selective adsorption of heavy or noble metal, enzyme immobilization for biocatalysis and immobilization of large chelating groups [20].

This material is distinguished from MCM-41 because of its larger diameter pores, ranging from 4.6 to 30 nm, the thicker pore walls and consequently higher thermal stability, and the mechanical and chemical resistance properties making it a preferable choice for use as a catalyst [17,21].

1.6 Functionalization of mesoporous silicas via one-pot synthesis (co-condensation) and post-synthesis modification (grafting)

The synthesis of mesoporous silica is accomplished using a template-forming agent, a long chain surfactant assembled into micelles at a specific surfactant concentration in aqueous solution known as critical micelle concentration (CMC). These amphiphilic molecules assemble in polar solvents forming a hexagonal array of cylindrical micelles in which the hydrophobic tail grouped in the center and the hydrophilic head on the surface. These micelles serve as template agents for the subsequent polycondensation of inorganic silicate precursor, such as tetraethyl orthosilicate (TEOS). Some silicas, for instance SBA-15, require further thermal treatment on an autoclave to rigidify the backbone forming an organic-inorganic composite. When this composite is calcined, the template is removed leaving only the porous network [22] (Figure 6).

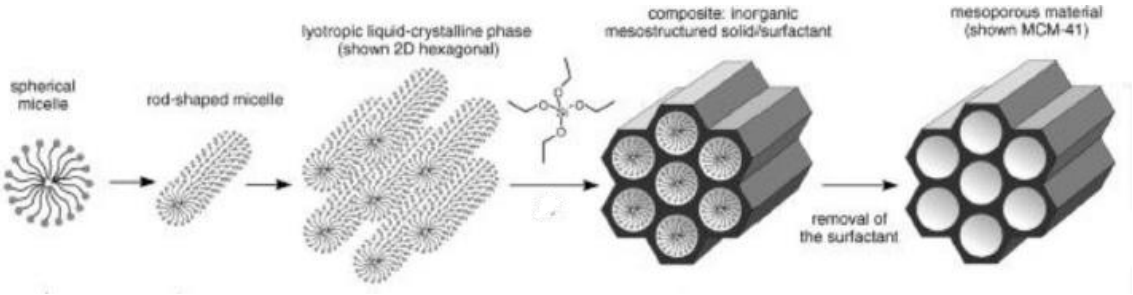

Figure 6 - Synthetic process of mesoporous silicas (retrieved from 22).

The backbone which make up the silicas can be regarded as polymers of silicic acid, consisting of an interlinked SiO_4 tetrahedra, the surface structure consists in either a siloxane group with the oxygen on the surface, or a silanol group. The silanols, illustrated in Figure 7, can be isolated or free where the surface silicon has three bonds into the bulk structure and the fourth attached to a single hydroxyl group, the geminal silanols or silanediol group consisting of two hydroxyl groups that are attached to one silicon atom, or vicinal groups where two silanols share a hydrogen bond [23,24].

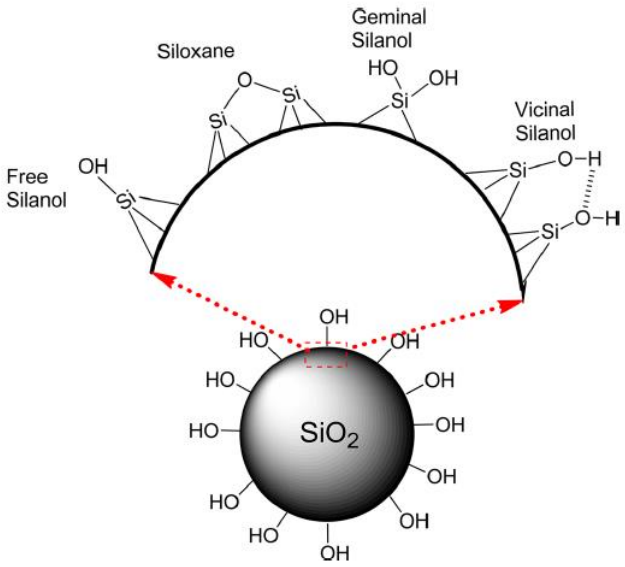

Figure 7 - Classification of silanol groups (retrieved from 24).

For the potential application of this materials in drug delivery it must be functionalized, since pure mesoporous silicas exhibit only silanol groups on the channel walls, and these silanol groups form weak intermolecular hydrogen bonds with drugs. For this purpose, functional groups are introduced on the surface of the porous networks (functionalization). This functionalization can be achieved via two different routes: one-pot synthesis (co-condensation) or post-synthesis modification (grafting) [20].

One-pot synthesis is a one-step method, in which the silica is formed and at the same time functionalized by co-condensation of inorganic silicate precursor (TEOS) and functional organosilane (siloxane). With this procedure, the loading and spatial distribution of the organic groups is better controlled only by selecting a desired silica/organosilane ratio. However, the binding site of the organosilanes may not be accessible, and some of them in fact may be buried within the walls of the silica and since, by this approach, the backbone has not been calcined it is susceptible to leaching and/or structural collapse, as illustrated in Figure 8 [25].

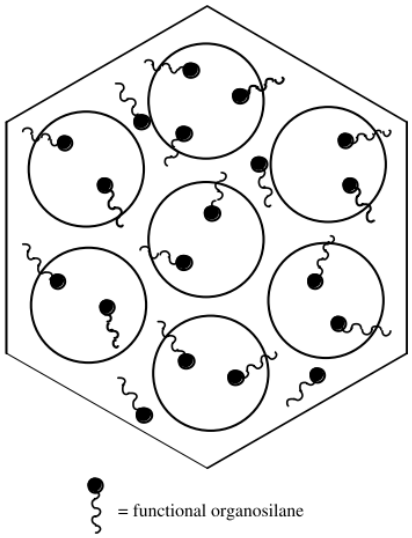

Figure 8 - Schematic showing functional organosilane distribuition via co-condensation (retrieved from 25).

Post-synthesis modification is the most common functionalization technique and is carried out with the treatment of the calcined mesoporous silica by the functional organosilane. This modification is called silylation and consists of covalently bond the functional group to the surface silanol groups. The major drawbacks of this method are the low control of loading and distribution of the functional groups, as illustrated in Figure 9 [26].

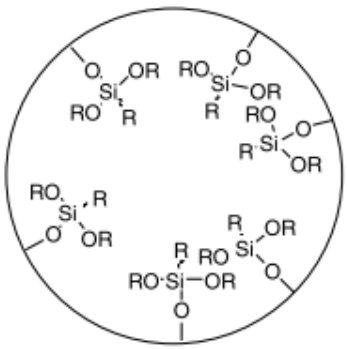

Figure 9 - Schematic showing the functional organosilane structure obtain from grafting (retrieved from 25).

1.7 Attenuated Total Reflectance Fourier Transform Infrared (ATR-FTIR) spectroscopy

Infrared radiation (IR) refers to part of the electromagnetic spectrum, between the visible and microwave regions. IR spectrum consists of infrared radiation being absorbed by an organic molecule and converted into energy of molecular vibration and rotation. This absorption is quantized resulting in a spectrum of absorbance or transmittance in function of the wavenumber.

Transmittance (T) is the ratio of the radiant power transmitted by a sample to the radiant power incident on the sample and absorbance (A) is the base 10 logarithm of the reciprocal of the transmittance [27].

In FTIR spectroscopy a mathematical Fourier transform is necessary to convert the raw data into the IR spectrum, and ATR is a technique which enables samples to be examined directly in the solid or liquid state without additional preparation. ATR operates by quantifying the changes that occur in an internally reflected infrared beam when in interaction with a sample [28].

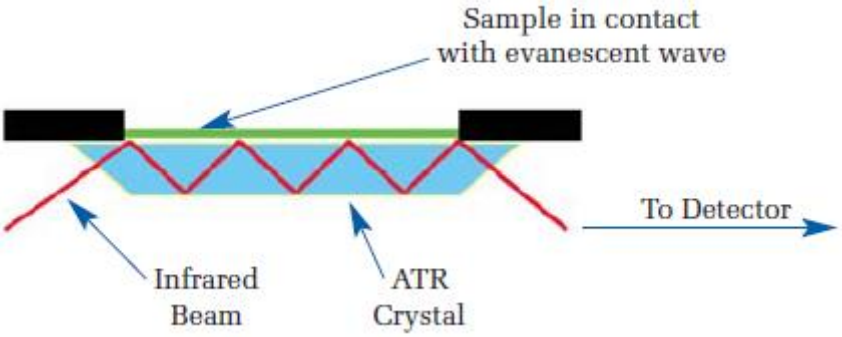

Figure 10 - Representation of ATR system (retrieved from 28).

ATR-FTIR consists of an infrared beam being directed to a crystal at a certain angle, creating a wave that extends beyond the crystal into the sample, that must be held in contact with the crystal (Figure 10). In regions of the infrared spectrum the sample absorbs energy, disturbing the wave which is detected in the opposite end of the crystal by a detector that generates the infrared spectrum [28].

1.8 Adsorption and desorption isotherms

Porous materials have received extensive interest for their sieving properties resulting from their pore structure, isolated or interconnected pores that may have similar or different shapes and sizes. Their pore shape can be defined by three basic models: cylindrical, ink-bottled or slit-shaped pores. Porous materials are also defined in terms of their adsorption-desorption properties, described quantitatively by an adsorption-desorption isotherm obtained from the amount of gas adsorbed by the material at a fixed temperature as a function of pressure, illustrated in Figure 11.

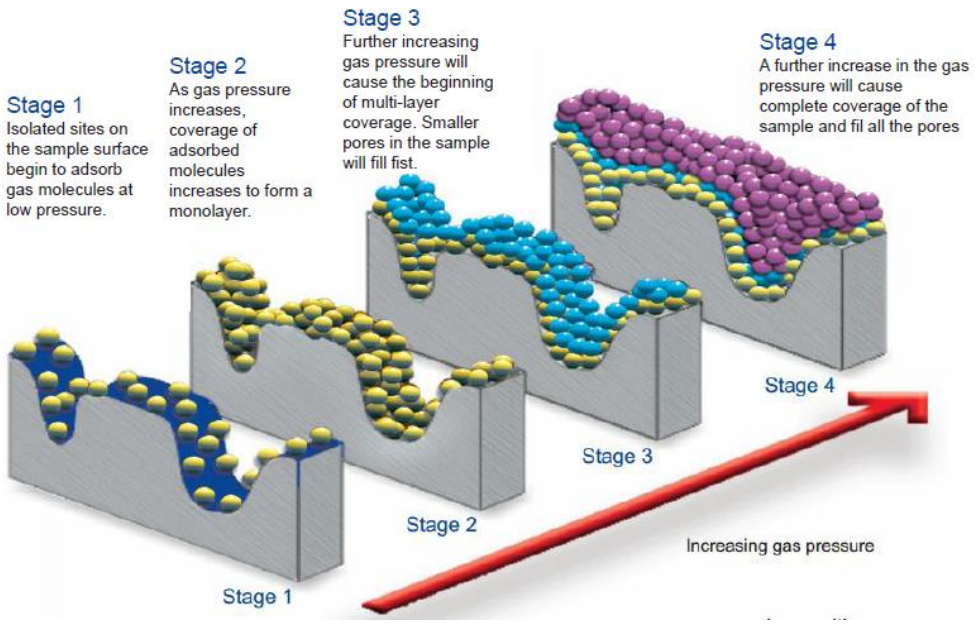

Figure 11 - Schematic of the adsorption stages. Desorption stages being the inverse (retrieved from 29).

The IUPAC classification of isotherms (Figure 11) reflects the connection between porosity and sorption (adsorption and or desorption) through six types of isotherm that are characteristic of microporous (type I), nonporous or macroporous (types II, III and VI) or mesoporous adsorbents (types IV and V) [17].

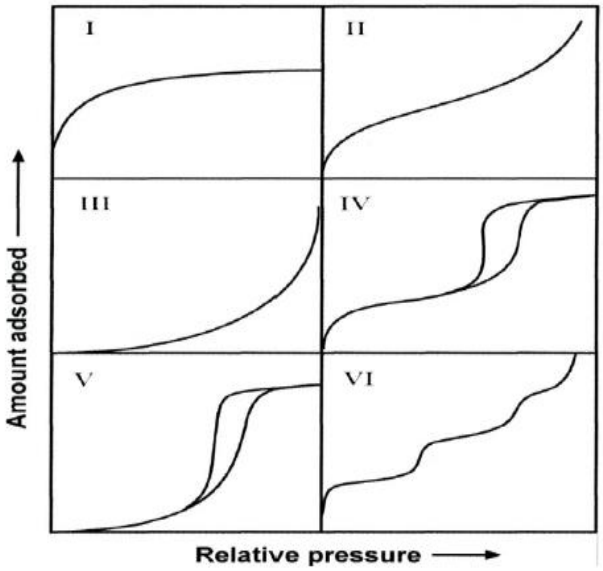

Figure 12 - The IUPAC classification of adsorption and desorption isotherms, with hysteresis in types IV and V (retrieved from 30).

In Figure 12, type IV and V isotherms exhibit adsorption hysteresis. The IUPAC classification of the adsorption hysteresis (Figure 13) correlate the shape of the hysteresis loop with pore shape (size distribution and pore geometry) of the mesoporous material. Type H1 is

associated with porous materials consisting of well-defined cylindrical-like pore channels or agglomerates of approximately uniform spheres. Type H2 describes materials that are often disordered where the distribution of pore size and shape is not well defined and indicate bottleneck constrictions as well. Type H3 hysteresis designates materials that have slit-shaped pores which are observed in non-rigid aggregates of plate-like particles. Finally, type H4 hysteresis are often associated with narrow slit pores [17].

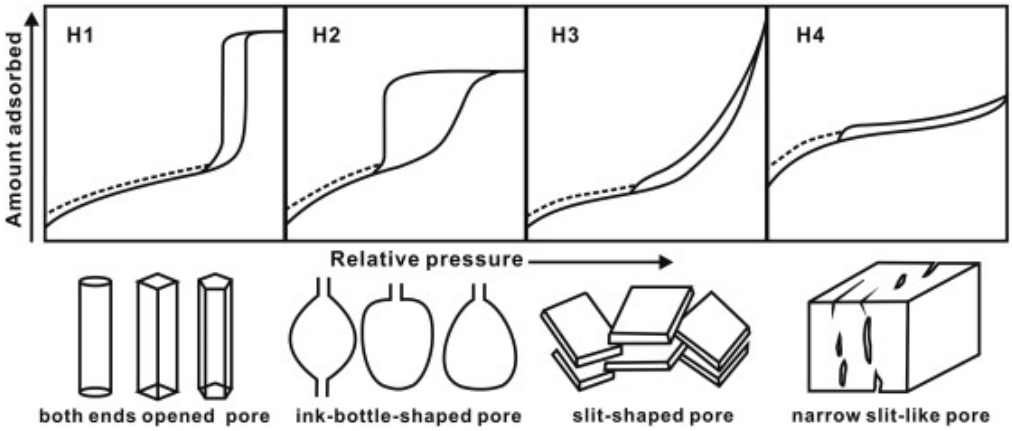

Figure 13 - The IUPAC classification of adsorption hysteresis loops and respective pore shape (retrieved from 30).

1.9 Solid state Nuclear Magnetic Resonance (ssNMR) spectroscopy

Solid state NMR spectra can provide a similar type of information obtained from solution NMR spectra through the application of special techniques such as magic-angle spinning (MAS) and cross-polarization (CP). MAS technique consists on the rotation of the sample about 54.74° with respect to the external magnetic field, diminishing the anisotropic dipolar interactions or orientation-dependent interactions that broaden the peaks on solid state spectra. The CP technique consists of transferring the polarization from abundant nuclei, such as proton, to rare nuclei in order to enhance the signal from the noise, discriminating against nucleus far away from the protons [31,32].

Solid state NMR experiments employing MAS, with or without CP are a reliable technique for quantitatively characterize the nature of various solid surfaces, in particular that of amorphous silica [32]. ssNMR measurements present direct information on the local environment of different structural units, making this technique a more sensitive method for studying from the alkyl chain attachment to solid state characterization of the confined pharmaceuticals. ^{29}Si NMR spectroscopies are used to probe the surface species in addition to the degree of cross-linking of the alkyl silanes. ^{13}C NMR spectroscopies are used to acquire further information about the alkyl

chain attachment to the mesoporous silica as well as the pharmaceutical interaction with the silica network [33–35].

A typical ^{29}Si MAS spectrum of silica materials present three signals between -92 and -110 ppm, represented in Figure 14. The peak at -92 ppm corresponds to geminal silanol sites (Q^2), the peak at -101 ppm is assigned to isolated silanol sites (Q^3) which may be either single (isolated silanols) or hydrogen bonded (vicinal silanols), while the signal at -110 ppm reflects surface polymerized groups, surface siloxanes (Q^4) [32,34].

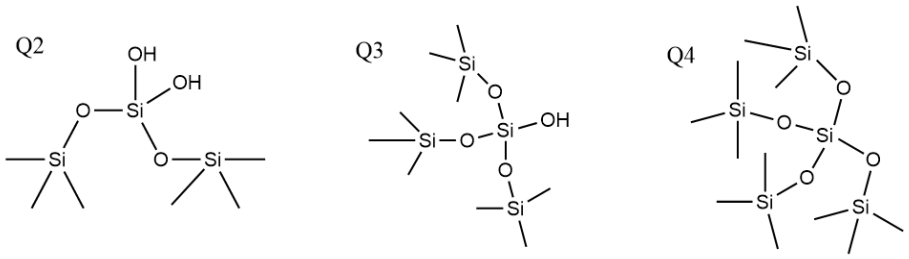

Figure 14 - Chemical structure of Q^n Si sites in silica.

The comparison of unmodified with surface modified samples reveals a significantly reduction in intensity of Q^2 and Q^3 sites peaks and a substantially increase in Q^4 intensity, upon surface modification. These redistributions of silicon sites intensity are due to the reactions of surface silanols groups with the siloxanes [32,34].

The attachment and cross-linking of the alkyl chains on the mesoporous silica surface are classified from the T^1, T^2 and T^3 sites (Figure 15) between -45 and -70 ppm. T^1 and T^2 sites refer to a partial cross-linking at -45 and -60 ppm, respectively, indicating an incomplete hydrolysis of the methoxy groups, and T^3 signals correspond to a complete cross-linking around -70 ppm [34].

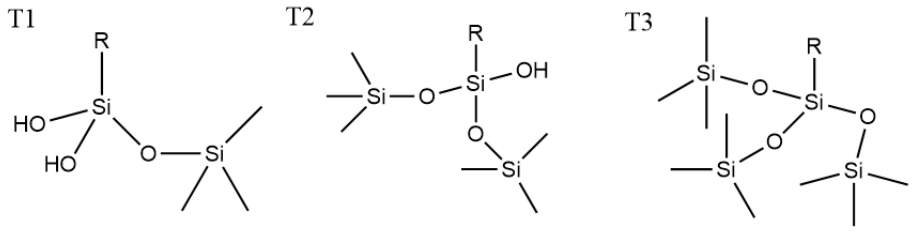

Figure 15 - Chemical structure of T^n Si sites.

Therefore, ^{29}Si NMR data, as shown in Figure 16, is analyzed according to the chemical shift for the Q^n and T^n sites. Where Q designates the presence of four oxygen first neighbors around a Si atom and T the presence of three oxygen first neighbors. The exponent n, from 0 to 4, the number of Si second neighbors [36].

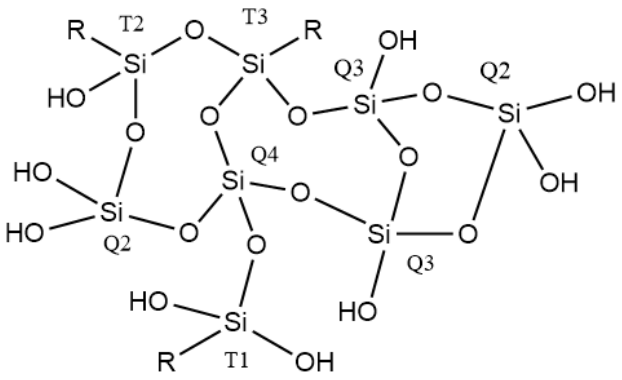

Figure 16 - Schematic representation of Q^n and T^n Si sites on a silica network.

1.10 Thermogravimetric analysis (TGA)

Thermogravimetric analysis (TGA) is an essential technique used to characterize materials for various applications, as environmental, pharmaceutical and petrochemical. TGA technique consists of the monitorization of the substance mass as a function of temperature or time as the sample is subjected to a controlled temperature program in a controlled atmosphere. The instrument consists of a precision balance that resides in a furnace (Figure 17) where the sample pan is heated or cooled, and the sample mass is monitored during the experiment. The environment inside the furnace is controlled by a sample purge gas, inert or a reactive gas, that flows over the sample and exits through an exhaust. These techniques precision offers the possibility to quantify losses of water, solvent, plasticizer, decarboxylation, pyrolysis, oxidation, decomposition, weight percentage filler, amount of metallic catalytic residue remaining on carbon nanotubes and weight percentage ash [37].

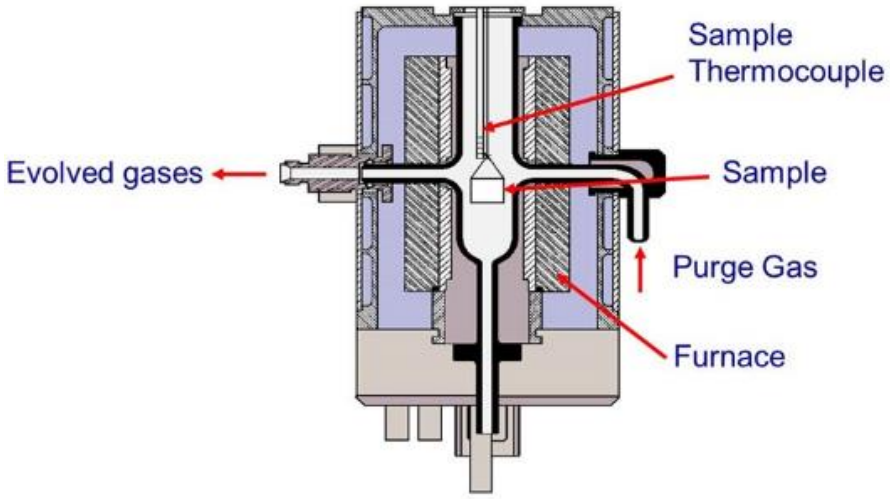

Figure 17 - Representation of TGA system (retrieved from 38).

1.11 Differential Scanning Calorimetry (DSC)

Differential scanning calorimetry is frequently the technique employed for thermal analysis of pharmaceutical compounds. This technique can provide detailed information about both physical and energetic properties of a substance, since other techniques don't have the ability of obtaining this information as accurately, easily or quickly. DSC consists of a two-pan configuration and measures the energy differences between the sample and the reference, providing quantitative information about exothermic, endothermic and heat capacity changes as a function of temperature and time [39].

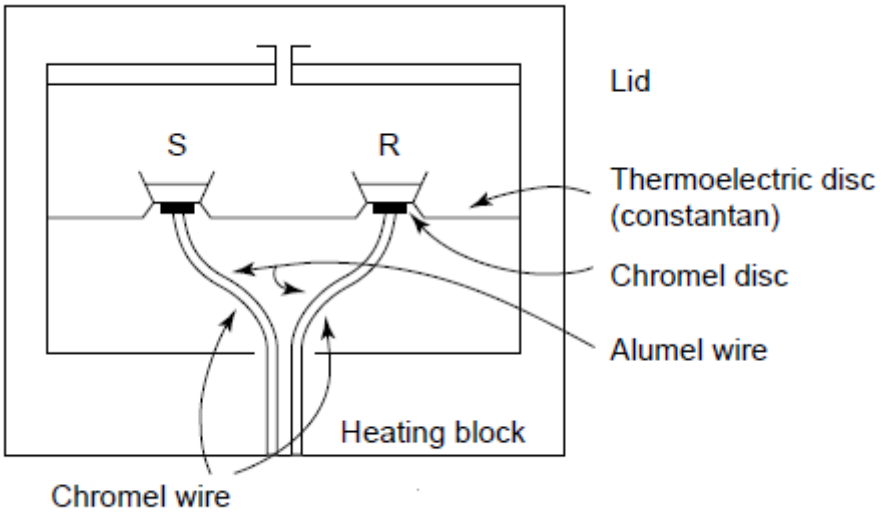

Figure 18 - Schematic diagrams of a heat-flux differential scannign calorimetry cells (retrieved from 39).

Heat flux DSC's operate with a single furnace where both sample and reference pans are heated at a constant rate ($\Delta T/\Delta t$) via a constantan thermoelectric disk, which is electrically heated (Figure 18). Heat flow ($\Delta Q/\Delta t$) is proportional to the difference in output of the two thermocouple junctions. Samples are analyzed in small metal pans designed for optimal thermal conductivity and minimum reaction with the samples. Sample pans may be open, pin-hole, crimped or sealed. The reference pan has an identical configuration though filled with an inert material, as air. The samples sizes common for pharmaceutical materials are 1-3 mg and should be accurately weighed at the start and end of each experimental run to obtain quantitative estimates of energetic parameters, such as heat capacity and enthalpy of fusion and crystallization. The sample compounds can exhibit enthalpic transitions, such as melting, crystallization and glass transitions [39].

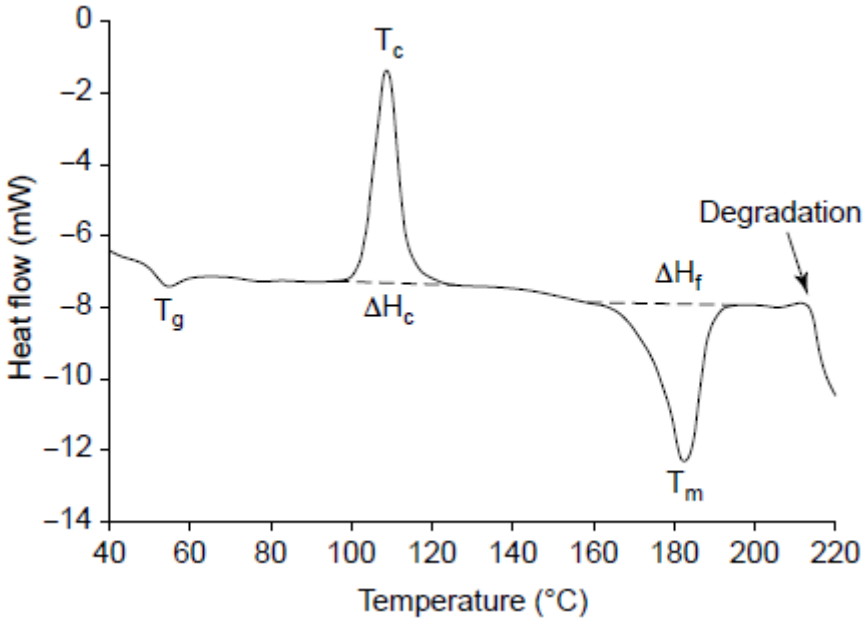

Figure 19 - Differential scanning calorimetry scan showing the glass transition temperature (T_g), recrystallization exotherm temperature (T_c) and enthalpy (ΔH_c), melting endotherm temperature (T_m) and enthalpy (ΔH_m) and degradation. Exothermic transitions are up (retrieved from 39*).*

Profile plots such as Figure 19 are obtained through the track of the starting temperature, heating rate, and heat flow, by the computer that records the difference in heat flow between the reference pan and the sample pan. The slope of the curve is the rate of heat capacity change, ΔCp⁄Δt. The heat flow may be divided by the heating rate to obtain a value for heat capacity and with knowing the mass of the sample can be obtained the specific heat capacity [40].

$$\frac{\frac{\Delta Q}{\Delta t}}{\frac{\Delta T}{\Delta t}} = \frac{\Delta Q}{\Delta T} = C_p \ (J\ °C^{-1}) \qquad \textbf{Equation 1}$$

$$\frac{C_p}{m} = c_p \ (J\ g^{-1}\ °C^{-1}) \qquad \textbf{Equation 2}$$

The glass transition, a second order transition since it has no latent heat associated, is characterized by a change in heat capacity, which is seen as a change in the baseline. Using the coordinates of two points ($T_{g\ onset}$ and $T_{g\ endset}$) and Equations 1 and 2, DSC can compute the glass transition temperature ($T_{g\ midpoint}$) and an accurate heat capacity of the glass transition.

The melting endotherm can be described by the onset temperature (T_o), the temperature where the transition starts to deviate from the baseline, the extrapolated onset melting temperature (T_e) that represents the intersection between the extrapolated baseline prior to the transition with the extrapolated leading edge of the transition and the peak temperature (T_m). The

enthalpy of fusion (ΔH_m) is obtained dividing the area of the endothermic transition (Equation 3) by the heating rate and the mass of the sample (Equation 4).

$$\frac{\Delta Q}{\Delta t}\,\Delta T = Area_{endo\ transition}\ (mW\,°C) \qquad \textbf{Equation 3}$$

$$Area_{endo\ transition} \Big/ m\frac{\Delta T}{\Delta t} = \Delta H_m\ (J/g) \qquad \textbf{Equation 4}$$

2 Materials and Methods

2.1 Synthesis of MCM-41

The synthesis of MCM-41 was prepared following the method described by Grün et al [18].

N-octadecyltrimethylammonium bromide (C_{18} TMABr) was used as template. Firstly, 2.56 g of the template was dissolved in 120 g deionized water to yield a 0.055 mol L^{-1} solution. To this solution was added 9.5 g of aqueous ammonia (25 wt%, 0.14 mol) and stirred for 2.5 h. While stirring, 10 g TEOS (0.05 mol) was slowly added, dropwise. The mixture was stirred for 1 h at room temperature, then the white precipitate was vacuum filtered and washed with 300 mL of deionized water. After drying at 100 ºC for 18 h, the sample was calcined at 550 ºC (heating rate of 1 ºC min^{-1}) in air and kept at this temperature for 5 h.

2.2 Synthesis of SBA-15

The synthesis of SBA-15 was performed according to Gao et al [41].

The triblock copolymer Pluronic P_{123} (poly (ethylene glycol)-block-poly (propylene glycol)-block-poly (ethylene glycol)) was used as the template. Firstly, 2.0 g of the template was dissolved in 60 mL of 2 M aqueous HCl and 15 mL of deionized water and the solution was left the solution under stirring for 1 h. Then 4.4 g of TEOS were added dropwise, at room temperature, and the mixture was stirred at 40 ºC for 24 h. Then the solution was transferred to an autoclave and kept at 100 ºC for another 24 h. Finally, the resulting precipitate was vacuum filtered, washed with 900 mL of deionized water, air dried and calcined at 500 ºC in air (heating rate of 10 ºC min^{-1}) and kept at this temperature for 5 h.

2.3 Post-synthesis modification

Different modifications were accomplished using methyltrimethoxysilane and chlorotrimethylsilane as functional organosilanes.

The functionalization with methyltrimethoxysilane was based on the procedures described in literature [42,43].

A solution of 150 mL dry toluene and 10 mL methyltrimethoxysilane was added to 1 g of template-free synthesized MCM-41 in nitrogen atmosphere to avoid the presence of water in the reaction. This solution was stirred and heated to 80 ºC, held for 6 h, and stirred overnight at room temperature. The precipitate was vacuum filtered, washed with 100 mL of dry toluene and 50 mL of ethanol, and finally, it was dried at 100 ºC for 24 h.

1 g of template-free synthesized SBA-15 was added to a solution of 150 mL of dry toluene and 15 mL of methyltrimethoxysilane in a nitrogen atmosphere. This solution was stirred and heated to 80 ºC, held for 6 h, and stirred overnight at room temperature. The precipitate was vacuum filtered and washed with 100 mL of dry toluene and 50 mL of ethanol. Finally, was dried at 100 ºC for 24 h.

The functionalization with chlorotrimethylsilane was prepared using a similar procedure previously described [32].

0.5 g of template-free synthesized MCM-41 was soaked in a solution of 10 mL of dry toluene and 5 mL of chlorotrimethylsilane in nitrogen atmosphere at ambient temperature under stirring for 24 h. The mixture was washed with 50 mL of dry toluene and 150 mL of ethanol. Finally, the powder was dried at 100 ºC overnight.

2.4 One-pot synthesis

The synthesis of MCM-41 with co-condensation was prepared according to method described in [26].

N-octadecyltrimethylammonium bromide (C_{18} TMABr) and n-hexadecyltrimethylammonium bromide (C_{16} TMABr) were used as template. Firstly, 0.78 g of C_{18} TMABr and 0.70 g of C_{16} TMABr (0.002 mol) were dissolved in 336 mL deionized water. To these solutions was added 2.45 mL of a NaOH solution (2 M) and stirred for 2 h at room temperature. Then the temperature was raised to 80 ºC. While stirring, 3.5 mL of TEOS (0.018 mol) and 0.43 mL of methyltrimethoxysilane (0.02 mol) were slowly added, dropwise, and the mixtures were stirred for 2 h at 80 ºC. The obtained white precipitates were vacuum filtered and washed with 500 mL of deionized water and 100 mL of methanol. After drying at 100 ºC for 20 h. The removal of the templates was achieved by reflux of the product for 37 h in 100 mL of ethanol, at 90 ºC, vacuum filtered and washed with 300 mL of ethanol, followed by a second reflux in a solution of 5 mL HCl and 95 mL of methanol until all the template was removed. Finally, the product was dried at 100 ºC for 48 h.

2.5 Ibuprofen loading

Firstly, the mesoporous silicas required an activation where water molecules and any impurity were removed. The MCM-41 and MCM-41_{sil} were held at 150 ºC at vacuum pressure (1.6 or 3 mbar) for 8 h, by immersion of the glass cells in a paraffin bath and left cooling to room temperature. After this activation, the powdered silicas samples were loaded with ibuprofen by soaking them into a 2 mL of chloroform solution of ibuprofen under vacuum. Powder composites samples were recovered by drying under agitation for 120 h at room temperature. Hereafter the composites will be designated according the matrix in which ibuprofen is loaded as Ibu:MCM and

Ibu:MCM-41$_{sil}$. In Table 1 are displayed the quantities and weight ratio of silica samples and ibuprofen, yielding a 60% of total pores capacity.

Table 1 - Quantities and weight ration of unmodified and modified MCM-41 samples and ibuprofen for a yield of 60% of total pores capacity.

Samples	Silica (mg)	Ibuprofen (mg)	Weight ratio
Ibu:MCM-41	101.1	44.0	2.3:1
Ibu:MCM-41$_{sil}$	101.3	42.0	2.4:1

2.6 Characterization methods

Infrared spectroscopy was performed on a PerkinElmer Spectrum Two FT-IR equipped with UATR sampling accessory. All samples were scanned in the wavenumber range from 400 cm^{-1} to 4000 cm^{-1} with a resolution of 1 cm^{-1} and 16 scans.

N_2 adsorption-desorption analysis were performed to determinate the specific surface area employing the linear portion of Brunauer-Emmett-Teller (BET) method plots, the total pore volume through the density functional theory (DFT) model and pore diameter using the Barrett-Joyner-Halenda (BJH) desorption method.

Solid state ^{13}C MAS and ^{29}Si MAS NMR spectra were acquired in a 7 T (300 MHz) AVANCE III Bruker spectrometer operating respectively at 75 MHz (^{13}C) and60 MHz (^{29}Si), equipped with a BBO probehead. The samples were spun at the magic angle at a frequency of 10 kHz in 4 mm diameter rotors at room temperature. The ^{13}C MAS NMR experiments were acquired with proton cross polarization (CP/MAS) with a contact time of 1.2 ms, and a recycle delay of 2.0 s. The ^{29}Si MAS NMR spectra were obtained using a single pulse sequence with a 90° pulse of 4.5 μs at a power of 40 W, and a relaxation delay of 10.0 s.

Thermogravimetric analysis was performed with samples of 2-3 mg placed in open platinum pans and submitted to a gradual temperature increase of 5 °C min^{-1} from 25.6 to 400 °C for the native ibuprofen sample and to 550 °C for the MCM-41, MCM-41$_{sil}$ and respective composites samples. The thermogravimetric measurements were determined with a TGA Q500 instrument from TA Instruments Inc. under nitrogen atmosphere with a sample purge flow rate of 60 mL min^{-1}.

Differential scanning calorimetry experiments were carried out with a DSC Q2000 (native ibuprofen and silica) and a DSC Q1000 followed by DSC Q10 (composites), all from TA Instruments Inc., operated under a nitrogen atmosphere with a flow rate of 50 mL min^{-1}. DSC Q2000 was calibrated at 10 °C min^{-1} and DSC Q1000 and DSC Q10 were calibrated at 20 °C min^{-1}. Samples of 2-8 mg were encapsulated in Tzero (aluminum) hermetic pans with a Tzero hermetic lid. Native ibuprofen samples measurements were obtained from encapsulated aluminum pans with a pinhole pinhole to allow water evaporation. Samples were submitted to a

procedure of several cooling and heating runs between -90 to 120 °C carried out at various cooling and heating rates of 5, 10, 20 and 30 °C min^{-1}. For the MCM-41 and MCM-41_{sil} samples, the procedure consisted of several cooling and heating runs between -90 and 170 °C performed at a rate of 10 °C min^{-1}. For the measurements carried out with the composites, the first heating run from 25 and 50 °C performed at a rate of 20 °C min^{-1} and kept 1 h at 50 °C were obtained from open pans. Afterwards the sample pans were closed, transferred and submitted to several cooling and heating runs between -150 and 100 °C performed at a rate of 20 °C min^{-1}.

2.7 *In vitro* release studies

The release studies were accomplished in 100 mL of a phosphate buffer, pH 6.8, maintained at a constant temperature of 37 ºC under continuous stirring until saturation. 1 mL samples were withdrawn and at the same time 1 mL of fresh phosphate buffer was supplemented at specific intervals of 1, 3, 5, 10, 12, 15, 20, 30, 45, 60, 90, 120 and 180 min and measured using a Perkin-Elmer 400 UV-Vis spectrophotometer scanned from 400 to 200 nm. The absorbance readings were translated to the amount of ibuprofen using a calibration curve derived from the standard solutions from 1-18 µg/mL of ibuprofen in phosphate buffer (Equation 6).

$$Abs = 0.0473\ (\pm 0.0004\ mL\ \mu g^{-1}) * C_t\ (\mu g\ mL^{-1}) \qquad \textbf{Equation 6}$$

The calibration curve was calculated for three wavelengths of 273 [19,20,44,45], 264 [46,47] and 222 nm [48] and linearity was only obtained at 222 nm ($r^2 = 0.9882$). All measurements were performed in triplicate and standard deviations from the average values were calculated.

3 Results and discussion

3.1 Characterization of the post-synthesis modification of silica

The characterization of the post-synthesis modification was performed on the modified MCM-41 by grafting (MCM-41$_{sil}$) with the methyltrimethoxysilane (Figure 20) and compared with the template-free synthesized MCM-41 (MCM-41).

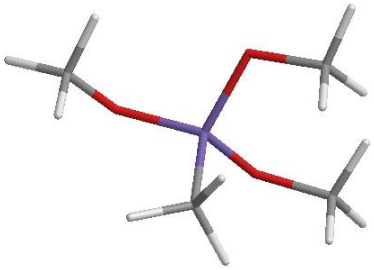

Figure 20 - Chemical structure of methyltrimethoxysilane.

The characterization was accomplished by ATR-FTIR analysis, N_2 adsorption-desorption, ^{29}Si MAS and ^{13}C CP/MAS ssNMR analysis.

ATR-FTIR spectra of MCM-41 and MCM-41$_{sil}$ are illustrated in Figure 21 and Figure 22.

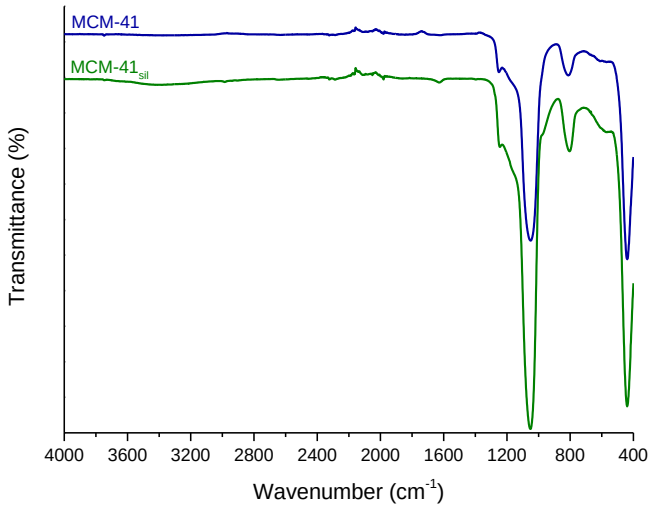

Figure 21 - ATR-FTIR spectra of MCM-41 MCM-41$_{sil}$. All the curves were vertically displaced for a better visualization. Wavenumbe range of 4000 to 400 cm^{-1}.

ATR-FTIR spectra (Figure 21) of both mesoporous silicas showed intense bands around 1300 and 1000 cm^{-1} typical of silica assigned as the asymmetric stretching of Si-O-Si groups, as

well as other bands relative to the bending vibrations of the Si-O groups at 806 cm^{-1}, the symmetric stretching modes of Si-O-Si groups at 567 cm^{-1} and the bridging bending modes of the O-Si-O groups at 439 cm^{-1} [49,50].

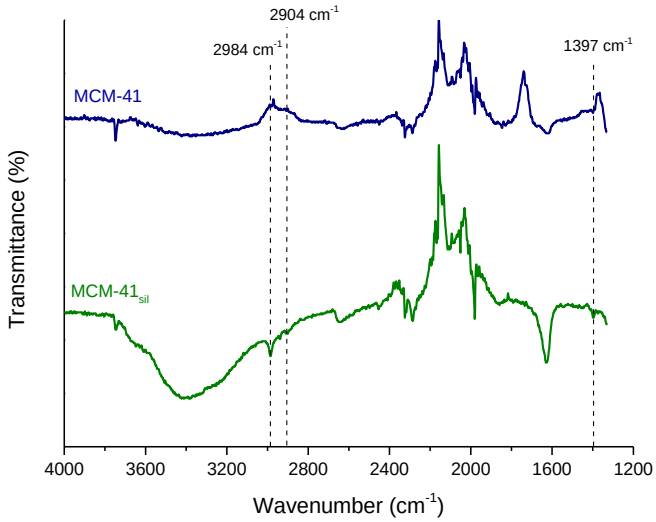

Figure 22 - ATR-FTIR spectra of MCM-41 and MCM-41$_{sil}$. All the curves were vertically displaced for a better visualization. Wavenumbe range of 4000 to 1200 cm^{-1}.

A close up of the ATR-FTIR spectra in the region between 4000 and 1200 cm^{-1} is shown in Figure 22. The band located at 3748 cm^{-1} is assigned to the stretching vibrational mode of free Si-OH groups, being detected in the unmodified silica, but also present in the matrix obtained by modification (green solid line). This is not a completely unexpected result, since the surface modification does not result in a full elimination of silanol groups. Furthermore, MCM-41$_{sil}$ spectrum showed an intense and broad band between 3670 cm^{-1} and 3013 cm^{-1} due to hydroxyl groups of adsorbed water. The presence of OH groups is also manifested by the detection of bands at 2939 cm^{-1}, 2655 cm^{-1}, 1624 cm^{-1}. By comparing spectra of both unloaded matrices, the signature of water is more evident in MCM-41$_{sil}$. As it will be seen later while analyzing thermogravimetric data, this is not a consequence of greater hydration in the modified silica but the fact that water molecules are more loosely bounded in the latter. This can be taken as a first indication that a lesser number of active sites (free silanol moieties) for water adsorption via hydrogen bonding exists in MCM-41$_{sil}$.

In relation to the organic functional groups the MCM-41$_{sil}$ spectrum showed bands at 2984 cm^{-1}, 2904 cm^{-1} and 1397 cm^{-1} assigned to either methoxy or Si-CH_3 groups [26,32,49,51], absent in the unmodified matrix, acting as a sign of efficient capping.

N_2 adsorption-desorption isotherms and pore size distribution are shown in Figure 23 and Figure 24, respectively. In Table 2 are summarized the textural properties such as specific surface area, pore diameter and total pore volume.

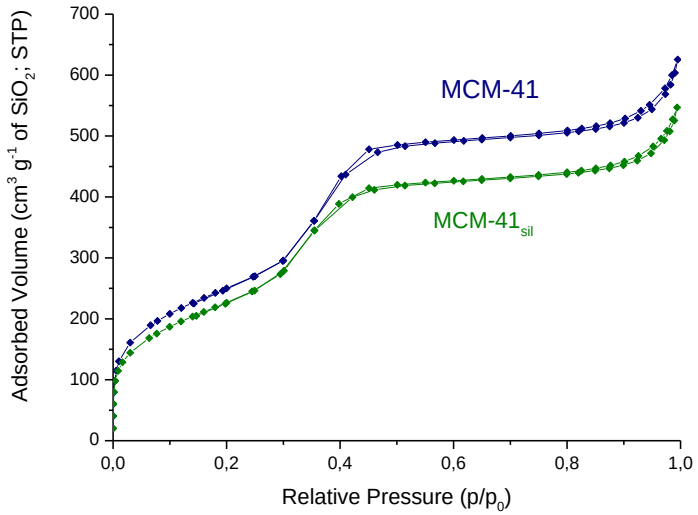

Figure 23 - Nitrogen adsorption/desorption isotherms of MCM-41 and MCM-41$_{sil}$.

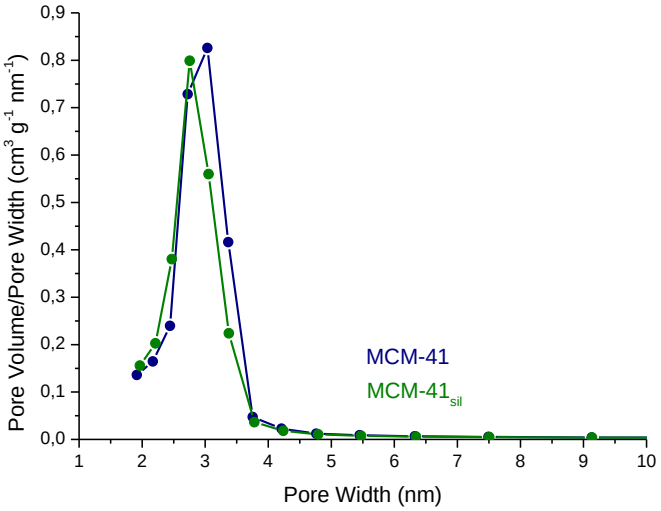

Figure 24 - Pore size distribution of MCM-41 and MCM-41$_{sil}$.

Both MCM-41 and MCM-41$_{sil}$ presented reversible type IV isotherms (Figure 23) typical of mesoporous materials [35,52]. MCM-41 isotherm showed a type H4 hysteresis loop that disappeared subsequently to modification. The isotherms showed in the 0.1-0.5 relative pressure range a typical step characteristic of a highly ordered mesoporous framework [19]. The comparison of both isotherms showed a slight decrease on the adsorbed volume from the MCM-41 to MCM-41$_{sil}$ caused by a small reduction of the specific surface[26] (see Table 2). Figure 24 presented, for both spectra, a narrow uniform mesopore size distribution, centered at 3.5 nm and 3.3 nm, respectively.

Table 2 – Textural properties of MCM-41 and MCM-41$_{sil}$.

Samples	Surface Area (m^2 g^{-1})	Pore Diameter (nm)	Total Pore Volume (cm^3 g^{-1})
MCM-41	926	3.5	0.73
MCM-41$_{sil}$	842	3.3	0.70

From the values presented on Table 2, a decrease of all three properties, specific surface area, pore diameter and total pore volume following modification was observed. This decrease resulted from less available space for adsorbed nitrogen proving the organic modification to some extent of the internal pore wall [19].

^{29}Si MAS ssNMR spectra of MCM-41 and MCM-41$_{sil}$ are represented in Figure 25. The deconvolution of the peaks was obtained applying the Gaussian functions, illustrated in Figure 26 and Figure 27.

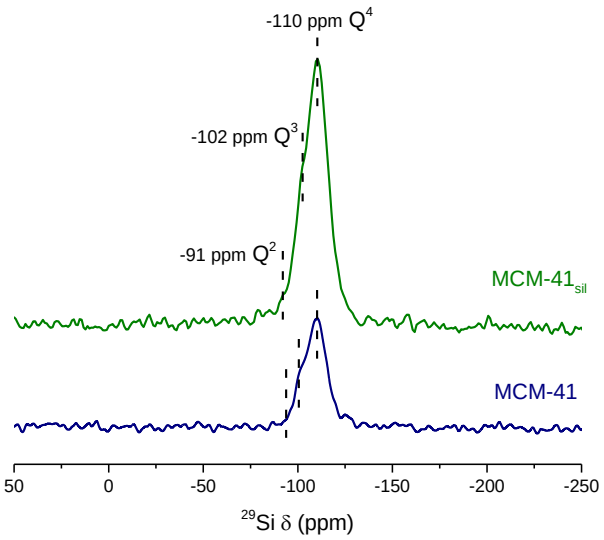

Figure 25 - ^{29}Si MAS ssNMR spectra of MCM-41 and MCM-41$_{sil}$.

The ^{29}Si MAS ssNMR spectra (Figure 25) exhibits different peaks between -91 and -110 ppm, which characterize the SiO_4 backbone of mesoporous silicas, originated from the hydrolysis of the inorganic silica precursor (TEOS) [36,53].

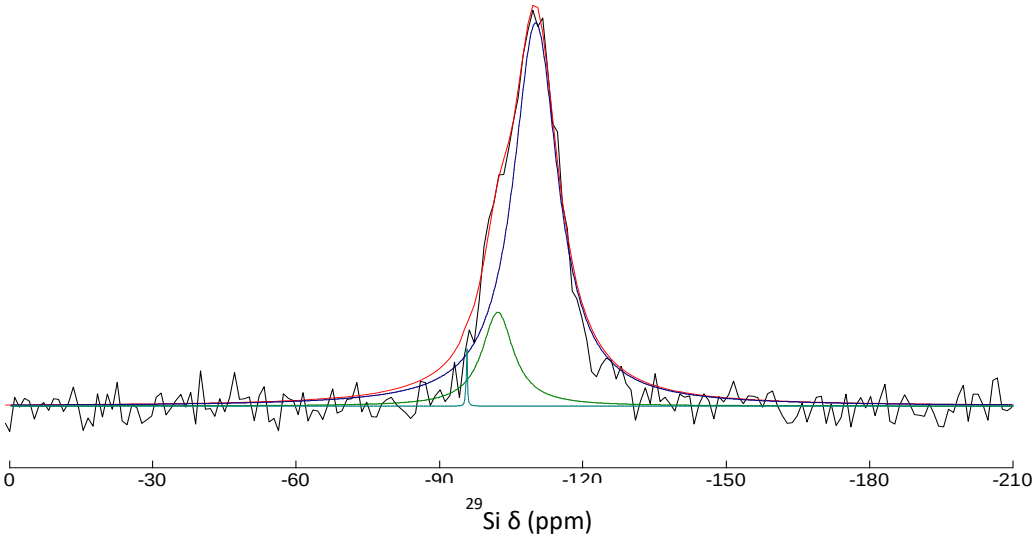

Figure 26 - Deconvolution of Q^n sites on the ^{29}Si MAS ssNMR spectra of MCM-41.

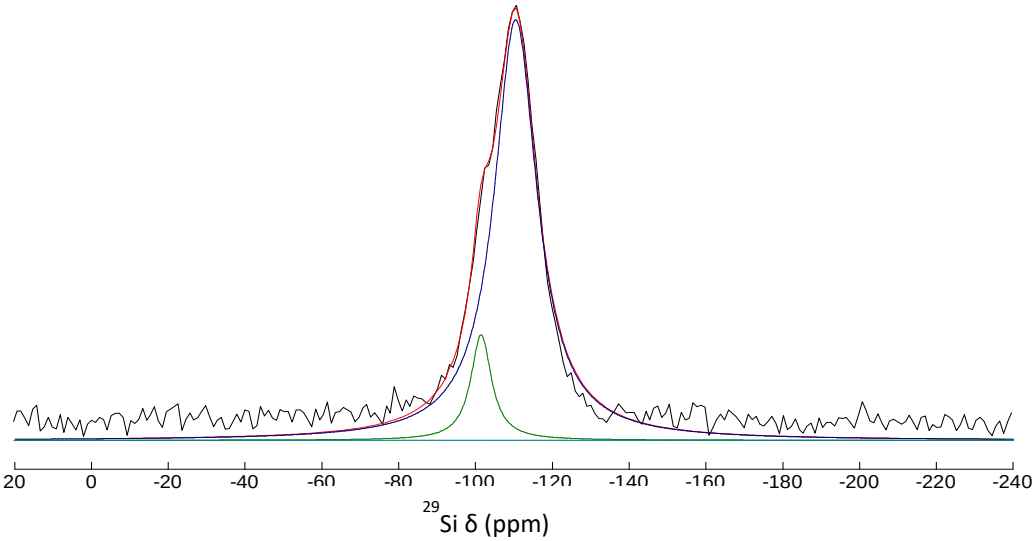

Figure 27 - Deconvolution of Q^n sites on the ^{29}Si MAS ssNMR spectra of MCM-41_{sil}.

^{29}Si MAS ssNMR spectra of both MCM-41 and MCM-41_{sil} (Figure 26 and Figure 27) correspond to an ensemble of peaks rather than a single were. Therefore, the global spectrum was deconvoluted in different individual Q^n contributions, each one quantified by a Gaussian/Lorentzian curve. The obtained ratio percentages are summarized with the respective chemical shifts of the peaks in Table 3.

Table 3 – Gaussian/Lorentzian ratio percentages and chemical shifts of the deconvoluted ^{29}Si MAS ssNMR spectra.

Samples	Q^2 sites	Q^3 sites	Q^4 sites
MCM-41	-95 ppm	-102 ppm	-110 ppm
	0.32%	14.56%	85.12%
MCM-41$_{sil}$	-93 ppm	-101 ppm	-110 ppm
	0.01%	10.72%	89.27%

Since Q^2 and Q^3 sites describes geminal and isolated or vicinal silanols (remember Figure 14), from Table 3 it is possible to observe a decrease of Si-OH sites and a subsequent increase of Q^4 sites of approximately 4% while comparing the unmodified silica with the modified one. This fact corresponds to a reduction of silanol groups available following modification, as expected with the incorporation of the methyl groups onto the silica surface [32,36,53].

^{13}C CP/MAS ssNMR spectra of MCM-41 and MCM-41$_{sil}$ are represented in Figure 28.

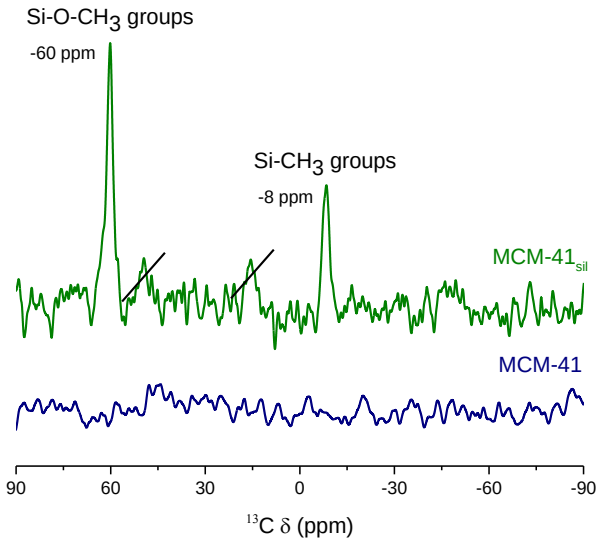

Figure 28 - ^{13}C CP/ MAS ssNMR spectra of MCM-41 and MCM-41$_{sil}$.

A distinctive aspect of the ^{13}C CP/MAS ssNMR spectra (Figure 28) is the presence of peaks below 75 ppm, implying the presence of sp^3-hybridised carbon atoms only[54]. This peak is only detected in the modified matrix, as expected due to the inclusion of methyl groups. This is corroborated by the detection of the peak centered at -8 ppm, which is assigned to methyl carbon atoms attached to silicon (Si-CH_3), implying that methyl groups were incorporated on the silica network [53]. The peak at 60 ppm indicates methoxy groups bound to silicon (Si-O-CH_3). This observation suggests either the presence of non-reacted siloxane or the existence of methoxy groups which are released during the hydrolysis of the siloxane that bound to the surface silanol groups [34]. Finally, both peaks around 15 and 50 ppm (indicated in the figure) correspond to the

methyl and methylene carbons of ethanol, respectively (CH_3CH_2OH) suggesting still the presence of this solvent, employed for modified silica washing, even after 24 h of drying [55].

3.2 Ibuprofen loading

Loading of ibuprofen into the mesoporous silicas MCM-41, modified MCM-41$_{sil}$ was confirmed through ATR-FTIR, N_2 adsorption-desorption, ^{29}Si MAS and ^{13}C CP/MAS NMR, DSC and TGA analysis.

ATR-FTIR analyses of MCM-41, MCM-41$_{sil}$ and composites as well as native Ibuprofen are illustrated in Figure 29.

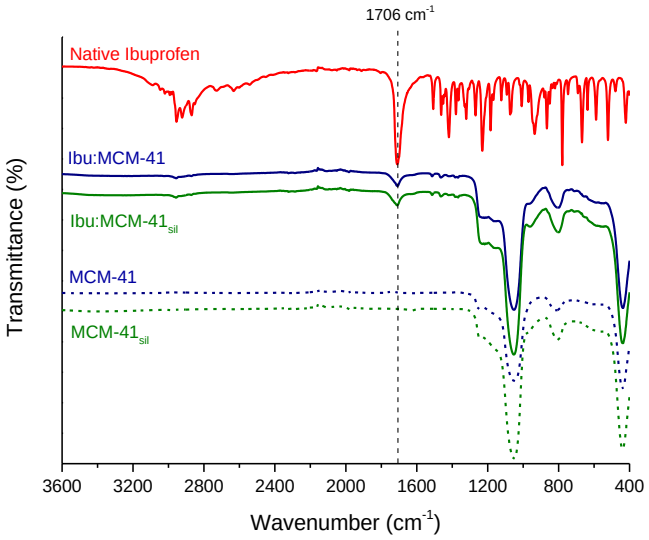

Figure 29 - ATR-FTIR spectra of MCM-41, MCM-41$_{sil}$, native ibuprofen and both composites (Ibu:MCM-41 and Ibu:MCM-41$_{sil}$). All the curves were vertically displaced for a better visualization.

The FTIR spectra (Figure 29) showed the presence of ibuprofen in the composites, Ibu:MCM-41 and Ibu:MCM-41$_{sil}$. The FTIR spectrum of pure crystalline ibuprofen (native ibuprofen) contains a characteristic band at 1706 cm^{-1} that corresponds to the carbonyl stretching vibration in hydrogen-bonded dimers [35]. The FTIR spectra of the composites display a weakening of the drug inter-atomic bonds, by the broadening of the C=O band, which can be a consequence of : i) the restriction of stretching vibrational modes inside of the pores [47], ii) the changing in the physical state of the incorporated drug from crystalline to amorphous exhibiting a less organized structure [56] and iii) the dispersion in the silica matrix. Other ibuprofen vibrational stretching bands presented in the composites were between 2955-2869 cm^{-1} assigned to C-H vibrations on the alkyl groups, 1511 cm^{-1} and 1461 cm^{-1} attributed to C-C vibrational modes in phenyl ring and at 1371 cm^{-1} assigned to carboxylic groups [19,44,46]. The simultaneous detection of these characteristic bands in both native drug and composites, proof the presence of ibuprofen in the loaded matrices.

N_2 adsorption-desorption isotherms are shown in Figure 30. In Table 4 are summarized the textural properties such as specific surface area, pore diameter and total pore volume.

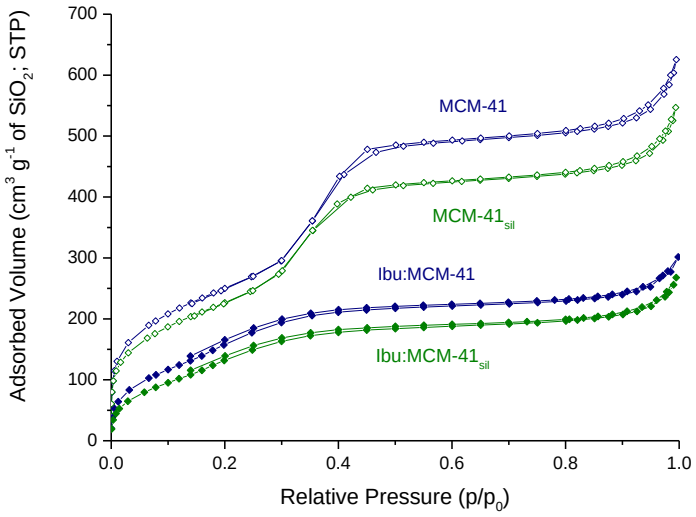

Figure 30 - Nitrogen adsorption/desorption isotherms of MCM-41, MCM-41$_{sil}$ and both composites.

Nitrogen isotherms of both Ibu:MCM-41 and Ibu:MCM-41$_{sil}$ still exhibited type IV isotherms with type IV hysteresis (Figure 30) [19,35]. The isotherms of both composites suffered a change in the typical step around 0.1-0.5 relative pressure range after loading indicating an nearly complete filling of mesopores with ibuprofen [35].

Table 4 – Textural properties of MCM-41, MCM-41$_{sil}$ and both composites.

Samples	Surface Area (m^2 g^{-1})	Pore Diameter (nm)	Total Pore Volume (cm^3 g^{-1})
MCM-41	926	3.5	0.73
MCM-41$_{sil}$	842	3.3	0.70
Ibu:MCM-41	653	3.2	0.36
Ibu:MCM-41$_{sil}$	549	3.3	0.25

From Table 4 was observed a decrease in all three properties, specific surface area, pore diameter and total pore volume on both composites. The significant decrease in the specific surface area and total pore volume resulted from ibuprofen adsorption inside the pores, indicating that ibuprofen is not blocking the pore entry [35].

^{29}Si MAS NMR spectra of MCM-41, MCM-41$_{sil}$ and both composites are represented in Figure 31.

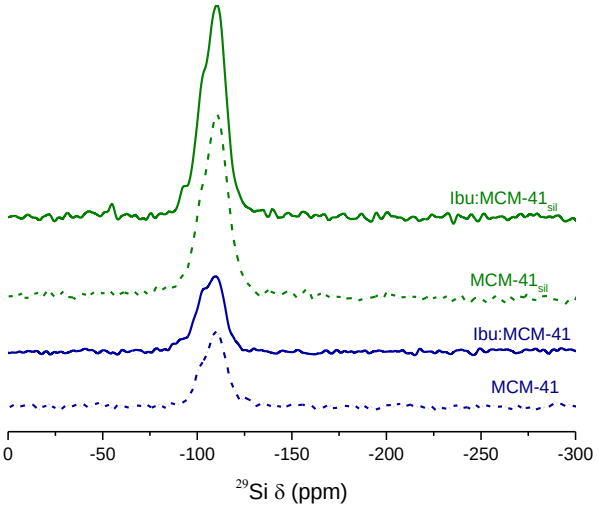

Figure 31 - ^{29}Si MAS NMR spectra of MCM-41, MCM-41$_{sil}$ and both composites.

The ^{29}Si MAS NMR spectra (Figure 31) showed the three characteristic peaks of Q^n sites, summarized in Table 5 after respective peak deconvolution illustrated in Figure 32 and Figure 33. In Figure 31, the spectrum of Ibu:MCM-41$_{sil}$ exhibited the Q^n sites at -92, -102 and -110 ppm in addition to a peak at -55 ppm which refer to T^2 groups. The existence of T^2 sites indicates an incomplete hydrolysis of the methoxy groups, resulting on a less efficient cross-linking of the alkyl chains on the surface of the silica [34]. The presence of T^2 sites exclusively on the Ibu:MCM-41$_{sil}$ rather than on both modified samples (MCM-41$_{sil}$ and Ibu:MCM-41$_{sil}$) may occur from the conditions carried out in the ibuprofen loading procedure, described formerly.

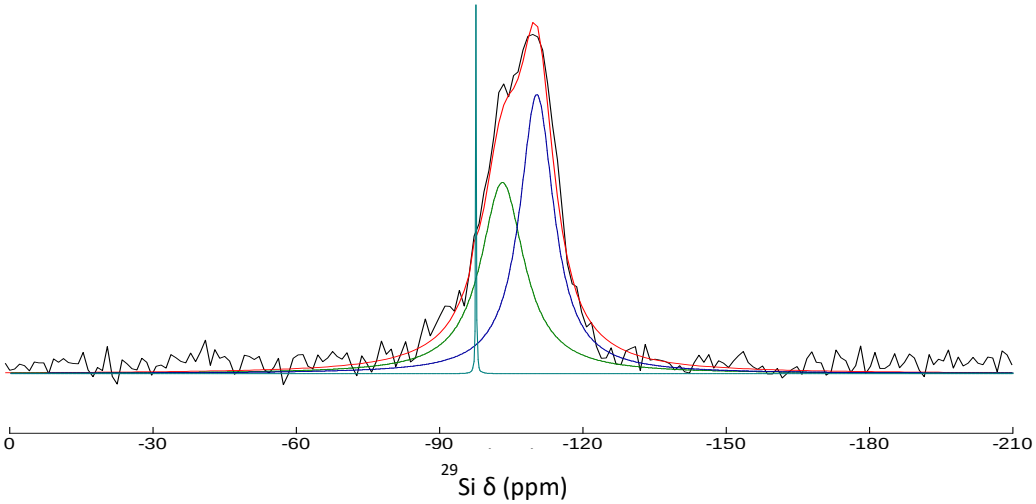

Figure 32 - Deconvolution of Q^n sites on the ^{29}Si MAS NMR spectra of Ibu:MCM-41.

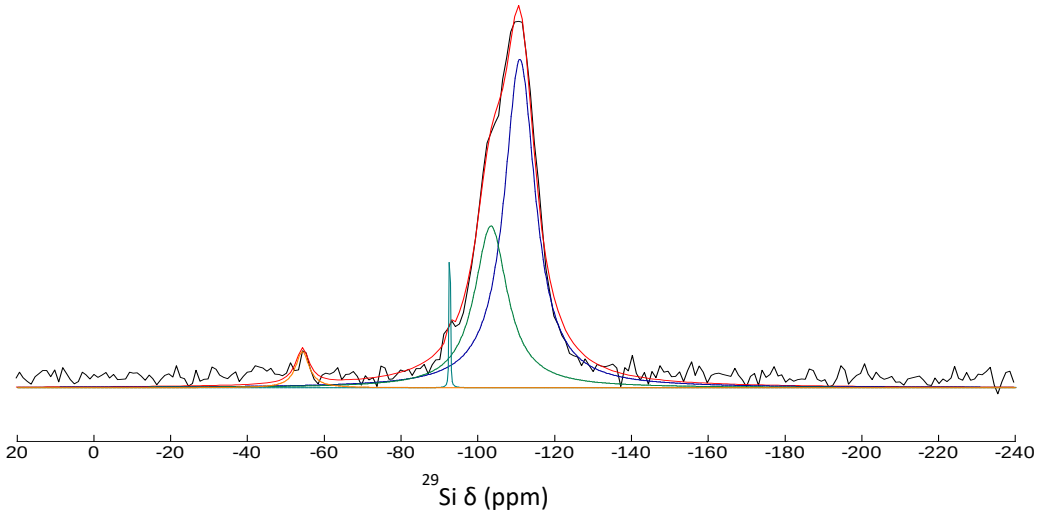

Figure 33 - Deconvolution of Q^n sites on the ^{29}Si MAS NMR spectra of Ibu:MCM-41$_{sil}$.

From Figure 32 and Figure 33, different Gaussian/Lorentzian ratio percentages were obtained, that are summarized with the respective chemical shifts of the peaks in Table 5.

Table 5 - Gaussian/Lorentzian ratio percentages and chemical shifts of the deconvoluted ^{29}Si MAS NMR spectra of MCM-41, MCM-41$_{sil}$ and composites. a) Not detected.

Samples	Q^2 sites	Q^3 sites	Q^4 sites	T^2 sites
MCM-41	-95 ppm	-102 ppm	-110 ppm	-
	0.32%	14.56%	85.12%	
MCM-41$_{sil}$	-93 ppm	-101 ppm	-110 ppm	a)
	0.01%	10.72%	89.27%	
Ibu:MCM-41	-97 ppm	-103 ppm	-110 ppm	-
	1.32%	45.94%	52.75%	
Ibu:MCM-41$_{sil}$	-92 ppm	-102 ppm	-110 ppm	-55 ppm
	1.23%	32.90%	62.84%	3.03%

Table 5 showed a decrease of Si-OH groups through the decrease in Q^2 and Q^3 sites, an increase of Q^4 sites and the presence of T^2 sites, according the reduction of silanol groups available after modification. The comparison of MCM-41, MCM-41$_{sil}$ and composites ratio percentages showed a significant decrease of Q^4 sites and consequent increase of Q^2 and Q^3 sites, indicating an increase of Si-OH groups possibly due to hydrolysis of the methoxy groups (see Figure 34) in certain conditions, as presence of water, or acidic conditions provided by the carboxylic acid group in ibuprofen, making it strongly acidic [57].

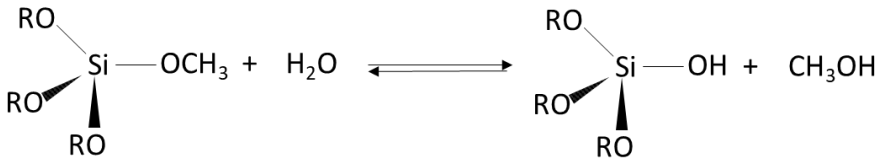

Figure 34 - Hydrolysis reaction of the methoxy groups.

^{13}C CP/MAS NMR spectra of MCM-41, MCM-41$_{sil}$ and both composites are represented in Figure 36 and Figure 37, respectively. ^{13}C CP/MAS NMR spectrum of native ibuprofen for comparison is illustrated in Figure 35.

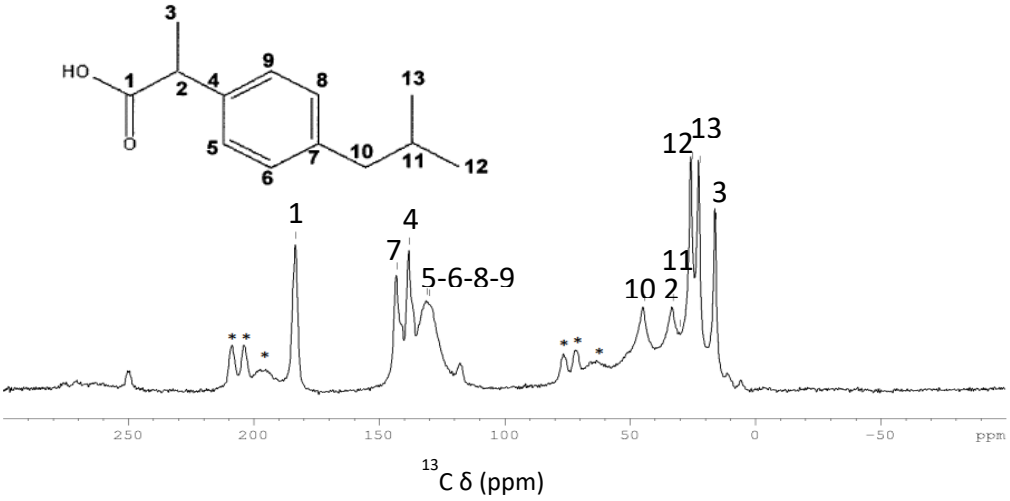

*Figure 35 - ^{13}C CP/MAS NMR spectrum of native ibuprofen. * Spinning side bands.*

From the comparison of ^{13}C solution and CP/MAS NMR spectra of native ibuprofen (Figure 35) and the ^{13}C CP/MAS NMR spectra of both composites (Figure 36 and Figure 37), peaks corresponding to ibuprofen molecules were detected, as well as those previously described related to methyl and methoxy groups bonded to the silica surface on the modified silica sample.

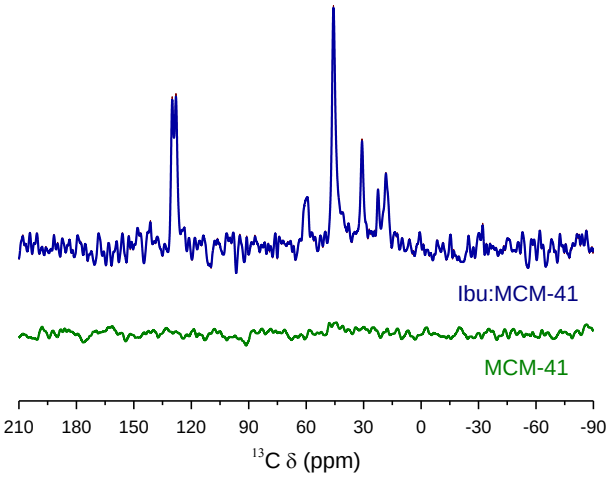

Figure 36 - ^{13}C CP/ MAS NMR spectra of MCM-41 and Ibu:MCM-41.

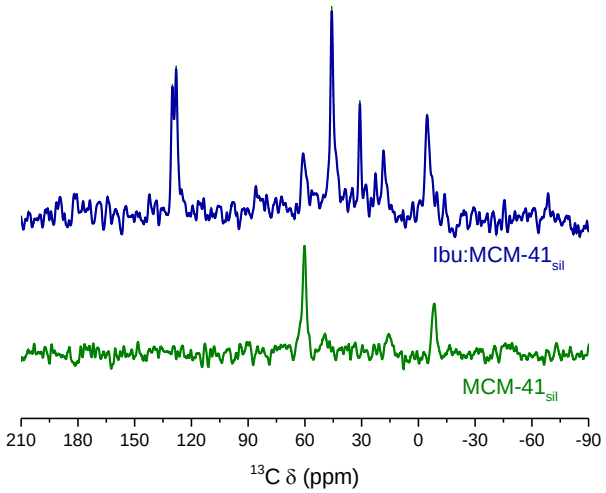

Figure 37 - ^{13}C CP/ MAS NMR spectra of MCM-41$_{sil}$ and Ibu:MCM-41$_{sil}$.

From Figure 36 and Figure 37 chemical shifts of both composites were obtained and summarized with the literature chemical shifts of native ibuprofen (Figure 35) in Table 6.

Table 6 – Assignments of ^{13}C CP/MAS NMR signals of native ibuprofen, Ibu:MCM-41 andIbu:MCM-41$_{sil}$. a) Not detected.

Samples	1	2	3	4	5-6-8-9	7	10	11	12	13
Native Ibuprofen	183.3	32.8	15.6	138.0	1301.1/130.8	143.0	44.3	30.0	25.3	22.2
Ibu:MCM-41	a)	45.7	18.9	a)	128.0/130.1	a)	45.7	30.6	22.1	22.1
Ibu:MCM-41$_{sil}$	a)	45.5	18.6	a)	128.0/130.1	a)	45.5	30.7	22.2	22.2

^{13}C CP/MAS NMR spectrum analysis of both composites (Table 6) showed a resemblance in number of peaks and a minor deviation of respective chemical shifts, confirming the presence of liquidlike ibuprofen in the silica pores [35].

Thermogravimetric analysis thermograms and respective derivative of native ibuprofen, MCM-41, MCM-41$_{sil}$ and composites are represented in Figures 38 and 39. A comparison of both unloaded silicas thermograms are illustrated in Figure 40. Figure 41 illustrates the derivative thermogram of the native ibuprofen and both composites.

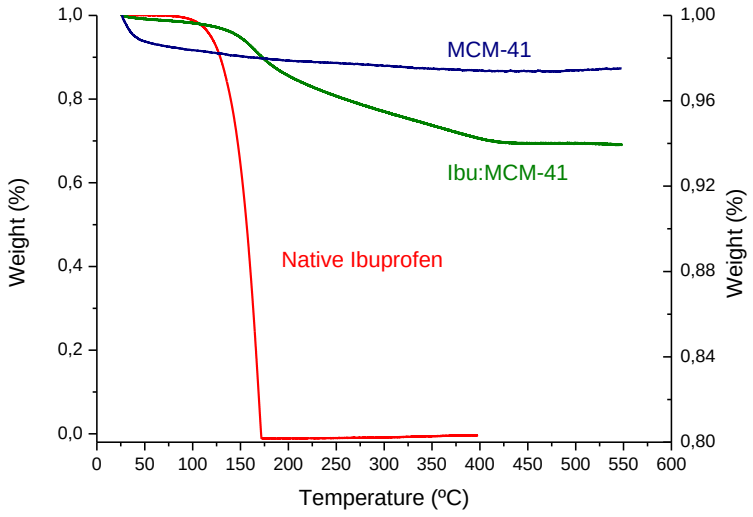

Figure 38 - TGA thermograms of native ibuprofen, MCM-41 and Ibu:MCM-41 obtained on heating at 5 °C min^{-1}.

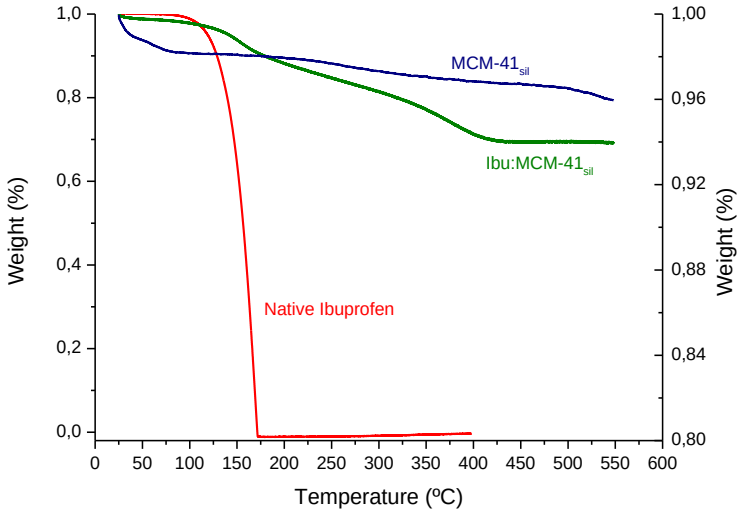

Figure 39 - TGA thermograms of native ibuprofen, MCM-41$_{sil}$ and Ibu:MCM-41$_{sil}$ obtained on heating at 5 °C min^{-1}.

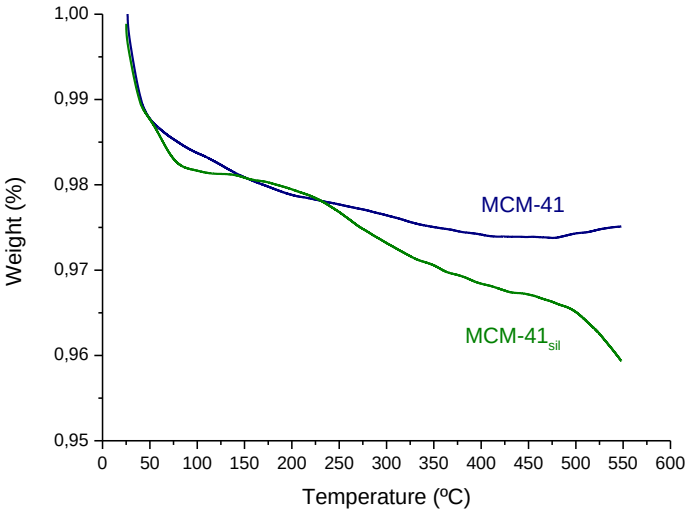

Figure 40 - TGA thermograms of MCM-41 and MCM-41$_{sil}$ obtained on heating at 5 °C min^{-1}.

The TGA thermograms (Figures 38 and 39) compares the decomposition of native ibuprofen with the composites and unloaded MCM-41 and MCM-41$_{sil}$. Concerning unloaded matrices, in general both MCM-41 and MCM-41$_{sil}$ presented a thermally stable profile; however, for the modified silica, a discontinuity around 350 °C was observed resulting from the decomposition of the organic functional groups. TGA thermograms (Figures 38 and 39) also allow to assess the water percentage in each mesoporous silica by the loss weight registered up to 150 °C; similar contents were found for both composites (Table 7). Interestingly, while analyzing thermograms of unloaded matrices (Figure 40), it was observed that higher temperatures were needed to remove water in the unmodified silica relative to the modified one. This corroborates

the ATR-FTIR analysis in which the surface modified silica showed weakly bounded water that in TGA is seen as being easily removed. Therefore, TGA assays are an additional tool that allows deducing that more tightly adsorbed water exits in MCM-41 due to hydrogen bonding with silanol groups.

Concerning ibuprofen decomposition, it took place in a single step with an onset nearly below 150 ^{0}C for the native drug, while in the composites it occurred in two steps around 200 °C and 400 ºC [58]. The loss weight allows the quantification of all species in the different materials as summarized in Table 7.

Table 7 - Water content, organic functional groups, ibuprofen loading, and filling obtained from the TGA thermograms of MCM-41, MCM-41$_{sil}$ and both composites.

Samples	Water (%w/w)	Organic Functional Groups (%w/w)	Ibuprofen Loading (%w/w)	Ibuprofen Filling (%v/v)
MCM-41	1.86	-	-	-
MCM-41$_{sil}$	1.91	2.03	-	-
Ibu:MCM-41	5.32	-	30.88	59.62
Ibu:MCM-41$_{sil}$	6.09	2.03	28.55	59.23

TGA thermograms (Figures 38 and 39) showed a weight loss of approximately 2-5% on every silica before 150 °C attributed to the removal of water or residual solvent. Figure 39 showed another weight loss of 2.03% at higher temperatures representative of the decomposition of the organic functional groups attached to the pore walls [45]. The ibuprofen filling was around 60% which coincides with the percentage intended in the loading calculations (Table 1).

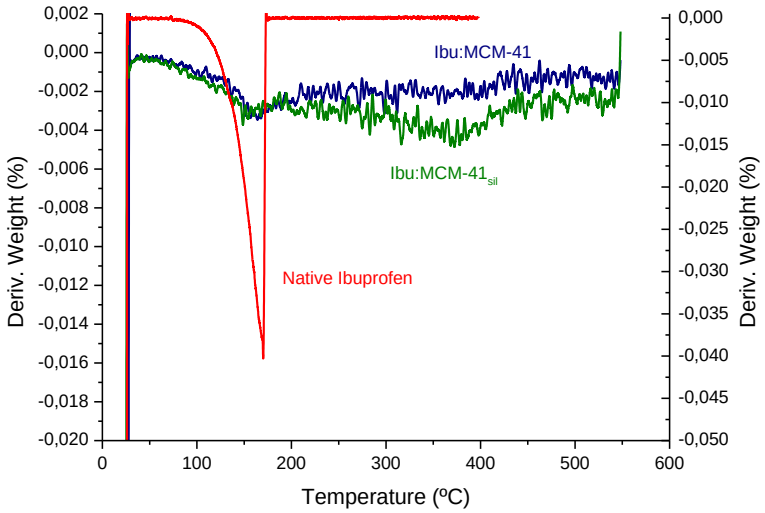

Figure 41 - TGA derivative thermograms of native ibuprofen and composites. obtained on heating at 5 °C min^{-1}.

The derivative thermogram (Figure 41) clearly shows that native ibuprofen presents a single peak decomposition, centered around 170 °C, whereas a two-peak profile is found for both composites, the major decomposition occurring at a higher temperature, around 370 °C. This suggests an enhancement of ibuprofen thermal stability inside the mesopores and a bimodal nature of its population due to i) bulk-like molecules and ii) ibuprofen molecules interacting with the pore walls in line with the thermal decomposition reported for the homologous naproxen incorporated in the MCM-41 [59].

Differential scanning calorimetric thermograms of native ibuprofen at various cooling and heating rates (5, 10, 20 and 30 °C min^{-1}) are represented in Figures 42, 43, 44 and 45, respectively. The DSC thermogram of mesoporous silica MCM-41 is demonstrated in Figure 46 and in Figures 47 and 48 are illustrated the DSC thermograms of both composites. Table 8 summarizes the glass transition temperature (T_g), cold crystallization exotherm temperature (T_c) and enthalpy (ΔH_c) and melting endotherm temperature (T_m) and enthalpy (ΔH_m) of native ibuprofen at the different cooling and heating rates as well as the both composites. Figure 49 illustrates the derivative thermogram of the native ibuprofen and both composites.

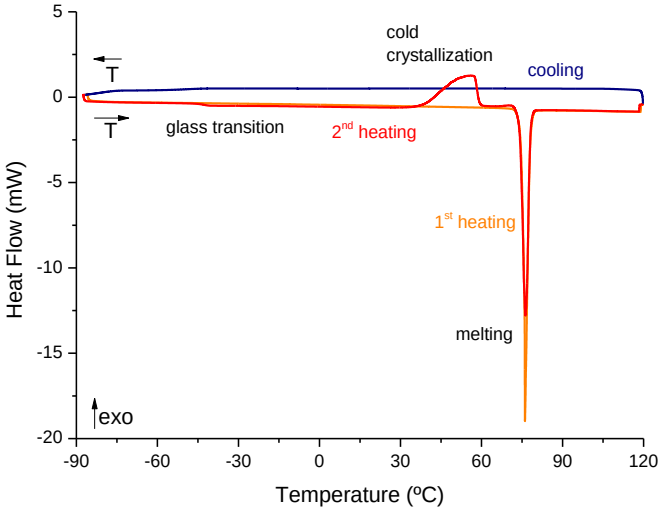

Figure 42 - DSC thermogram of native ibuprofen scanned at a cooling and heating rate of 5 °C min^{-1}.

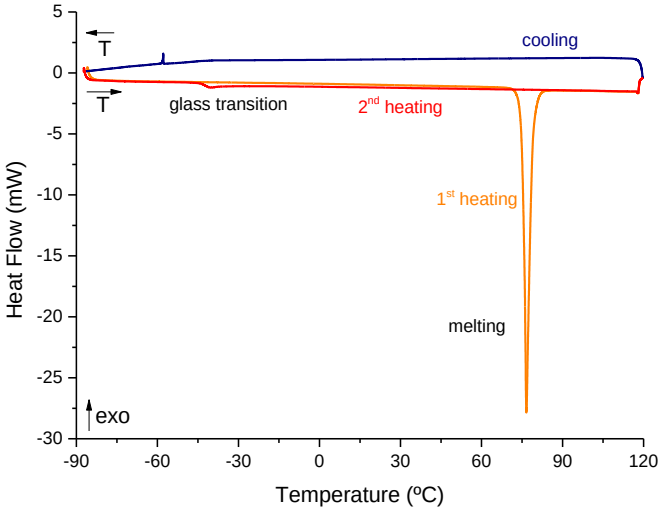

Figure 43 - DSC thermogram of native ibuprofen scanned at a cooling and heating rate of 10 °C min^{-1}.

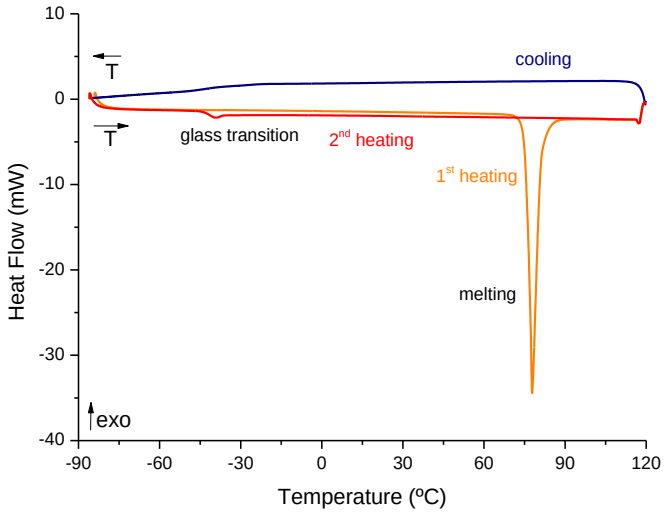

Figure 44 - DSC thermogram of native ibuprofen scanned at a cooling and heating rate of 20 °C min^{-1}.

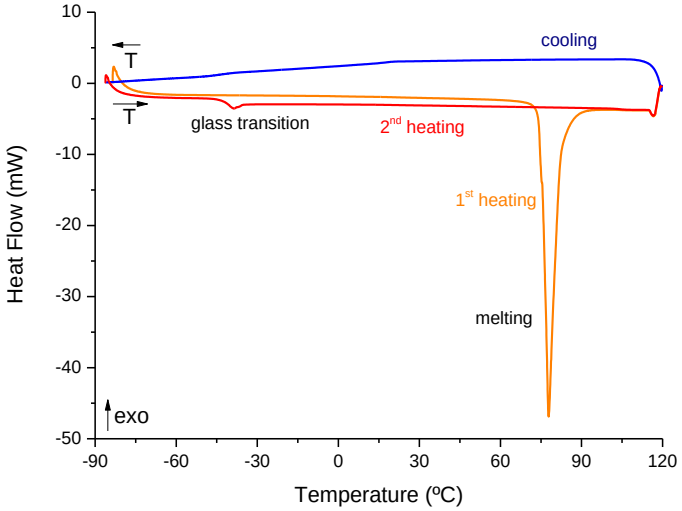

Figure 45 - DSC thermogram of native ibuprofen scanned at a cooling and heating rate of 30 °C min^{-1}.

The DSC thermograms for the native ibuprofen (Figures 42, 43, 44 and 45) showed sharp melting endothermic peak at the first heating run/scan around 77 °C indicating the melting of crystalline form of the drug [60]. At the following cooling run/scan the absence of a recrystallization exothermic peak and at the second heating run/scan the presence of glass transition around -41 °C and absence of melting peak implied the complete amorphization of native ibuprofen [47,48]. At a rate of 5 °C min^{-1} (Figure 42) a thermal phenomenon of cold crystallization and subsequent melting occurs at the second heating after glass transition, induced by the considerable number of crystal nuclei previously formed during the cooling step that resulted from the increase of

nucleation rate with the supercooling. From the comparison with higher cooling and heating rates (Figures 43, 44 and 45) was observed an elimination of the cold crystallization [61].

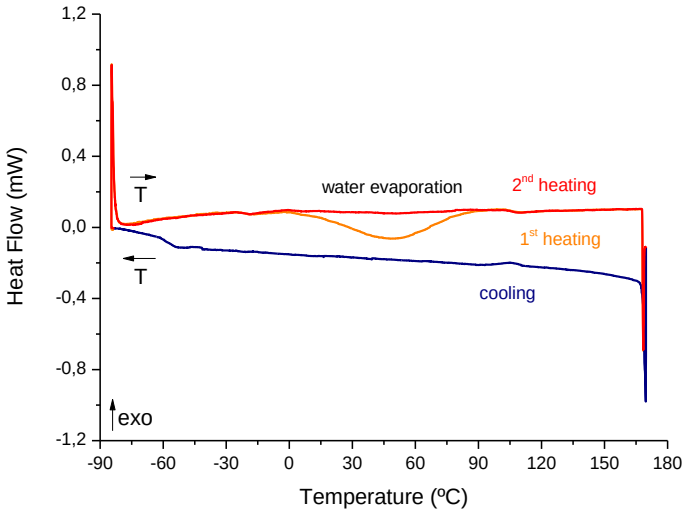

Figure 46 - DSC thermogram of mesoporous silica MCM-41 scanned at a cooling and heating rate of 10 °C min^{-1}.

The DSC thermogram of the mesoporous silica MCM-41 (Figure 46) showed only, at the first heating, a broad endothermic peak between 10 and 80 °C resultant from gradual release of water adsorbed on the external and internal surface of mesopores [49].

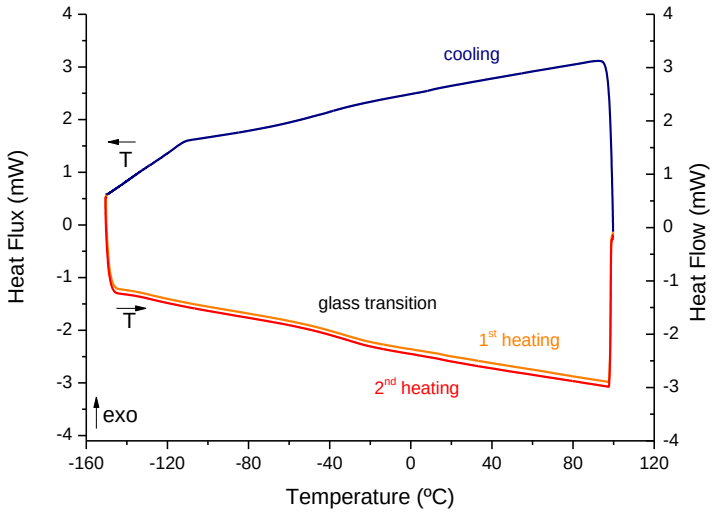

Figure 47 - DSC thermogram of Ibu:MCM-41 scanned at a cooling and heating rate of 20 °C min^{-1}.

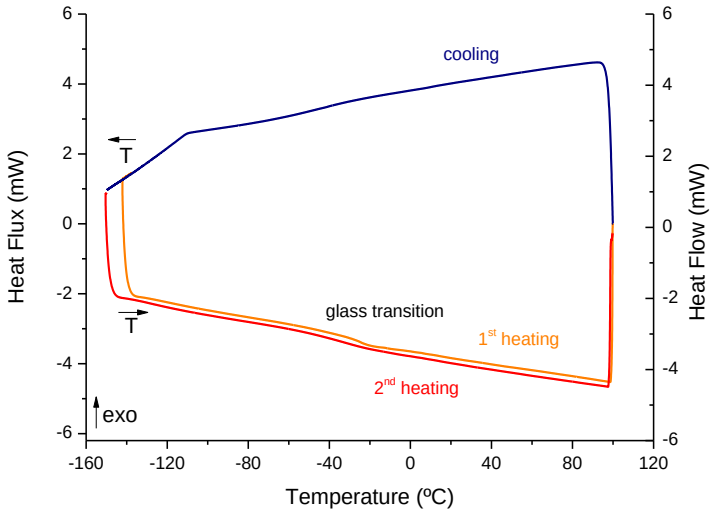

Figure 48 - DSC thermogram of Ibu:MCM-41$_{sil}$ scanned at a cooling and heating rate of 20 °C min^{-1}.

Both composites were firstly submitted to a drying procedure, described previously, and subsequently the DSC thermograms (Figures 47 and 48) were obtained where all the events are only due to the incorporated ibuprofen. In Figures 47 and 48 was observed a glass transition event as well as a complete disappearance of the ibuprofen melting peak implying the complete inclusion, supported by the smaller size of ibuprofen molecules (1.15 nm), and subsequent amorphization of the drug [35,47,49].

From Figures 42, 43, 44, 45, 47 and 48 were acquired the glass transition temperature ($T_{g\ midpoint}$), cold crystallization exotherm temperature (T_c) and enthalpy (ΔH_c) and melting endotherm temperature (T_m) and enthalpy (ΔH_m) of native ibuprofen at four different cooling and heating rates and of the composites and summarized at Table 8.

Table 8 - DSC thermogram properties of native ibuprofen and both composites. a) Values adjusted according the water lost and loading percentage.

Samples	$T_{g\ midpoint}$ (ºC)	ΔCp (J g^{-1} $ºC^{-1}$)[a)]	T_c (ºC)	ΔH_c (J g^{-1})	T_m (ºC)	ΔH_m (J g^{-1})
Native Ibuprofen						
5 ºC min^{-1}	-43.16	0.3908	56.25	74.7	76.09/76.29	126.8/108.5
10 ºC min-1	-41.33	0.4819	-	-	76.59	130.3
20 ºC min-1	-40.39	0.6010	-	-	77.81	125.3
30 ºC min-1	-40.19	0.6436	-	-	77.83	128.1
Ibu:MCM-41	-33.27	0.4230	-	-	-	-
Ibu:MCM-41_{sil}	-24.50	0.2159	-	-	-	-

The properties values obtained for native ibuprofen such as $T_{g,midpoint}$, ΔH_m and T_m (Table 8) are in agreement with the literature [60,62].

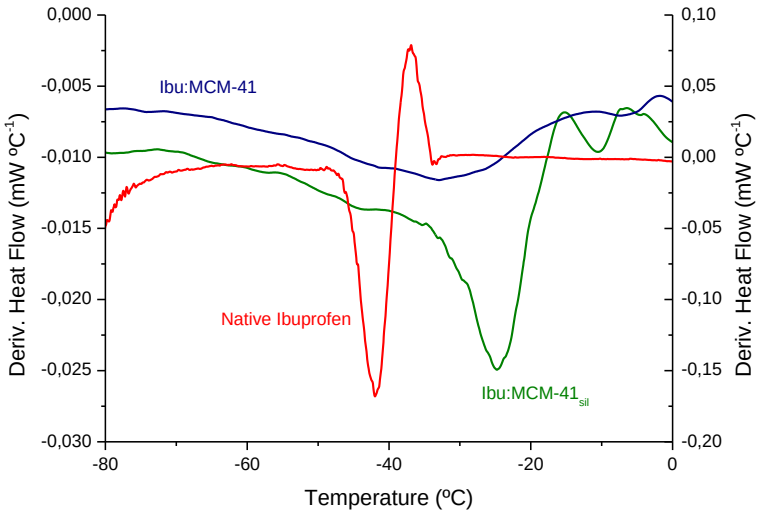

Figure 49 - DSC heat flow derivative thermogram of the first heating of native ibuprofen and the second heating of both composites. The primary axis refers to the native ibuprofen and the secondary to the composites.

The comparison of the heat flow derivative of the first heating of native ibuprofen and the second heating of both composites (Figure 49) showed that both composites present two populations, one around -40 °C corresponding to the glass transition temperature of native ibuprofen and the second at higher temperatures around -33 °C for Ibu:MCM-41 and -24 °C for Ibu:MCM-41_{sil}. This distinction between populations, more obvious in the surface modified composite, already seen in the derivative TGA analysis, imply a variation of the location of ibuprofen inside the mesopores. The first population, more bulk-like, embodies the ibuprofen that

makes no interactions with the silica surface by being located on the center of the pore. For contrary, the second population expresses the ibuprofen molecules that are hydrogen bonded with the surface of the silica resulting in more thermal stable molecules and so appearing at higher temperatures; again, in agreement with TGA results. The difference in temperatures of the second population of both composites conveys the idea of stronger interactions of ibuprofen in the pores with the surface of the modified sample. The more distinctive high temperature population in the modified silica is probably a consequence of the hydrolysis of methoxy groups in acidic conditions provided by the ibuprofen loading, resulting in Si-OH groups and free methanol. This provides an increase of the number of active sites for guest-host hydrogen bonding [57].

3.3 *In vitro* release studies and kinetics

The *in vitro* release profiles of the composites are illustrated at Figures 50 and 51, as well as the native ibuprofen dissolution profile for comparison.

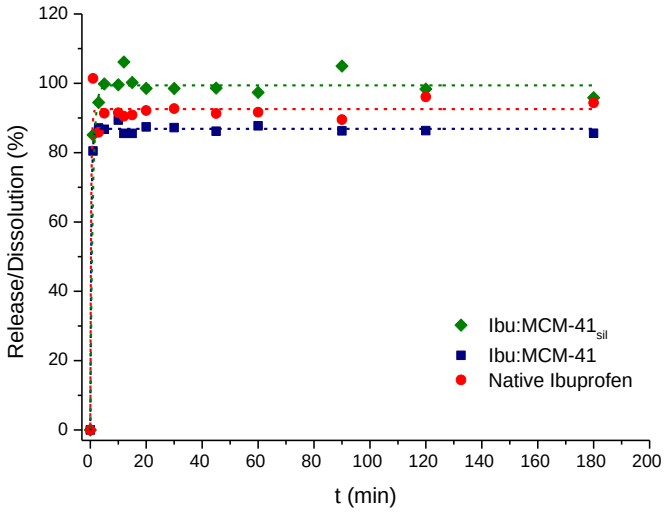

Figure 50 - In vitro release profiles of native ibuprofen and composites.

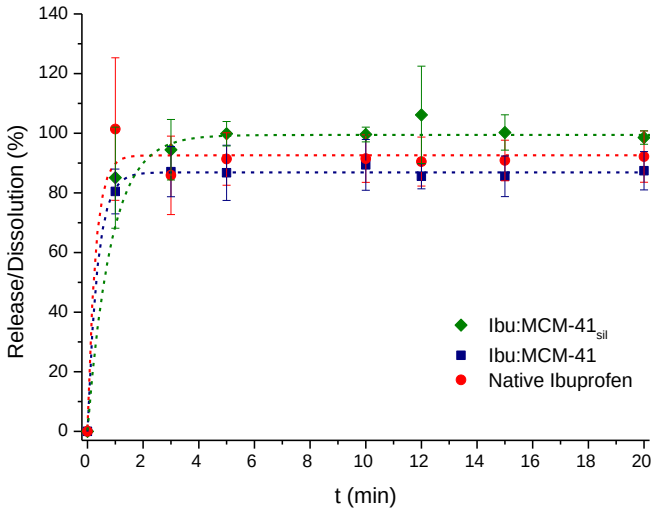

Figure 51 - In vitro release profiles of native ibuprofen and composites. Zoom on the burst release.

The release profiles of Ibu:MCM-41 and Ibu:MCM-41$_{sil}$ were similar between them and with the dissolution one (see Figure 50 and the scale up in Figure 51). Comparing the profiles of both composites with native ibuprofen, it was observed: i) a decrease of ibuprofen dissolution rate compared to the explosive release of native ibuprofen (identical to which is reported in literature [44]); ii) both composites achieve a plateau in the release trace that corresponds, respectively to 89.40% for Ibu:MCM-41 occurring after 3 min, and to 106.15% for Ibu:MCM-41$_{sil}$, after 12 min. Both composites showed an initial burst release of 90% of the maximum attained in the plateau region, probably due to drug molecules weakly entrapped inside the mesopores (Table 9); this is followed by a slow release attributed to the hydrogen-bonds interactions between ibuprofen molecules and the silanols present in the surface of the silicas [20,46].

Table 9 - Burst release profile and linear release rate of the composites. Burst percentages relative to the maximum released of 89.40 and 106.15 % of Ibu:MCM-41 and Ibu:MCM-41$_{sil}$, respectively.

Samples	Burst (%)	t_{burst} (min)	Linear release rate (% min^{-1})	Maximum release (%)	$t_{maximum\ release}$ (min)
Ibu:MCM-41	90.02	1	80.48	89.40	3
Ibu:MCM-41$_{sil}$	88.99	3	31.49	106.15	12

Several mathematical models, presented in Table 10, were used to study the mechanism of the ibuprofen release data (Figure 50) from the composites.

Table 10 - Mathematical models applied to study the ibuprofen released from the composites. Where F is the fraction of drug released up to the time t; k_o, k_f, k_H, $k_{1/3}$ and k_{K-P} are the rate constants of the mathematical models; n is the release exponent of the Korsmeyer-Peppas model [63].

Mathematical Model	Equation
Zero order	$F = k_0 t$
First order	$\ln(1 - F) = -k_f t$
Higuchi	$F = k_H t^{1/2}$
Hixon-Crowell	$1 - (1 - F)^{1/3} = k_{1/3} t$
Korsmeyer-Peppas	$F = k_{K-P} t^n$

Zero order model describes the drug release from several types of delivery systems such as matrix tablets for drugs with low solubility and osmotic systems, where drug release would be directly proportional to time [63]. First order model defines the release profile from delivery systems involving hydrophilic drugs dispersed in porous matrices, where drug release can be controlled by diffusion along the ordered array of the matrix and the drug would be release at rates proportional to the amount of drug remaining in the interior of the delivery system [19,63]. Higuchi model depicts the drug release from an insoluble matrix based on the Fick's Law, where the release occurs by the diffusion of drugs within the delivery system [45,63]. Hixson-Crowell's model applies to delivery systems whose drug release rate is proportional to the surface area of the system such as the erosion-dependent release systems [63]. Korsmeyer-Peppas explains the release of pharmaceutical polymeric dosage forms when the release mechanism is not well known or when more than one type of release phenomena was involved, applying only to the first 60% of the cumulative amount of drug release. This model used the release exponent (*n*) to characterize four different release mechanisms as Fickian-controlled diffusion (n=0.43), non-Fickian model or anomalous transport ($0.43<n<0.85$), Case-II transport or time-independent release kinetics (n=0.85) and Super Case II transport mechanism ($0.85<n\leq1$) [45,63].

In Table 11 and Table 12 are summarized for each composite the mathematical models parameters presented in Table 10, the squared correlation coefficients (R^2), the rate constant characteristic of each model (*k*) obtained after mathematical model fitting of the ibuprofen release data.

Table 11 - Parameters obtained with fitting of the mathematical models to the release data of the Ibu:MCM-41 sample.

Mathematical Model	R^2	*k*	*n*
Zero order	0.0067	0.0008 (h^{-1})	-
First order	0.9924	18.5106 (h^{-1})	-
Higuchi	0.0430	0.0472 ($h^{-1/2}$)	-
Hixon-Crowell	0.0236	0.0011 ($h^{-1/3}$)	-
Korsmeyer-Peppas	0.4786	0.2616 (h^{-n})	0.5

Table 12 - Parameters obtained with fitting of the mathematical models to the release data of the Ibu:MCM-41$_{sil}$ sample.

Mathematical Model	R^2	*k*	*n*
Zero order	0.0038	0.0009 (h^{-1})	-
First order	0.9846	1.8789 (h^{-1})	-
Higuchi	0.0386	0.0535 ($h^{-1/2}$)	-
Hixon-Crowell	0.0186	0.0012 ($h^{-1/3}$)	-
Korsmeyer-Peppas	0.5543	0.3005 (h^{-n})	0.5

As shown in Table 11 and Table 12, First order model gave the highest value of squared correlation coefficient (R^2), being the most suitable model to describe the ibuprofen release profile of both composites. From the comparison of the rate constant (*k*) value corresponding to the first order model for the Ibu:MCM-41 and Ibu:MCM-41$_{sil}$ samples was noted a substantial decrease of 90% in agreement to the significantly different values of the linear release rate (Table 9), corresponding to a meaningfully slower release rate after modification due to the hydrolysis of the methoxy groups.

4 Conclusions

The work here reported try to answer to a pharmaceutical industry demand for more water-soluble drugs, which was tried by amorphization through incorporation in a mesoporous matrix and, simultaneously, to provide a rational basis for the observed delivery profile in terms of guest-host interactions.

Ibuprofen, a nonsteroidal anti-inflammatory drug, was used as target material and unmodified and surface treated mesoporous inorganic silica matrices (100% Si), respectively, MCM-41 and MCM-41$_{sil}$, were used as hosts.

The work was preceded by the evaluation of the phase transformations of the native drug, also allowing to get familiar with differential scanning calorimetry (DSC). The as received ibuprofen shows a melting endothermic peak centered at T_m = 77 °C, which confirmed the crystalline state of the starting material. Upon cooling, the material avoided crystallization undergoing a glass transition that, in the subsequent heating, is detected with a midpoint temperature ($T_{g,midpoint}$) located between -44 and -40 °C; the shift was induced by the increase of the cooling/heating rate from 5 to 30 °C/min. Additionally, in the experiments carried out at a cooling/heating rate of 5 °C/min, although crystallization is circumvented during cooling, it occurs upon heating after devitrification - the so-called cold crystallization – followed by melting at T ~ T_m. By this thermal study it is concluded that the amorphization of native ibuprofen is easily accomplished, nevertheless it shows a tendency to recede to the more stable crystalline state, depending on thermal treatment. This reinforces the need of stabilization of the amorphous form that was done through incorporation inside a mesoporous matrix.

The study proceeded with the characterization of the MCM-41 mesoporous silicas having different surface chemical composition: a free-template synthesized (MCM-41) and a modified by grafting with methyltrimethoxysilane (silylation) (MCM-41$_{sil}$). The nitrogen adsorption-desorption analysis confirmed a narrow pore size distribution, centered at 3.5 nm and 3.3 nm, respectively for, MCM-41 and MCM-41$_{sil}$. The surface modification was validated through attenuated total reflectance Fourier transform infrared (ATR-FTIR), ^{29}Si MAS solid state nuclear magnetic resonance (ssNMR) together with ^{13}C CP/MAS ssNMR spectroscopy studies, being possible to conclude the presence and although partial attachment of the functional organosilane on the MCM-41$_{sil}$. Also, the decrease of surface area and pore volume, as observed by nitrogen adsorption-desorption analysis, reinforced the achievement of surface modification. Furthermore, ATR-FTIR gave evidence of a more loosely water in the modified matrix, while more strongly hydrogen-bonded water is detected in the untreated silica; this was confirmed by thermogravimetric analysis (TGA) since higher temperatures are needed to full remove water in MCM-41. These results were interpreted as a consequence of a reduction of silanol groups in MCM-41$_{sil}$ due to the surface treatment; since they are active sites for water adsorption, its reduction impaired the interaction with drug molecules via hydrogen bonding.

The drug loading was carried by capillarity under vacuum in both MCM-41 and MCM-41$_{sil}$. The ibuprofen loading on the composites, Ibu:MCM-41 and Ibu:MCM-41$_{sil}$, was confirmed by a set of experimental techniques such as ATR-FTIR, ^{29}Si MAS ssNMR jointly with ^{13}C CP/MAS ssNMR, DSC and TGA as well as nitrogen adsorption-desorption analysis that showed a significant decrease of pore volume. TGA analysis detected a two-step decomposition profile and a bimodal heat flux discontinuity was found by DSC. By calorimetry, the heat flux shows a discontinuity due to the glass transition around -40 °C, close to $T_{g,midpoint}$ of native ibuprofen, and a second step at higher temperatures, around -33 °C for Ibu:MCM-41 and -24 °C for Ibu:MCM-41$_{sil}$. So, by TGA and DSC it was concluded a presence of two different populations of ibuprofen molecules inside the mesopores, one more bulk-like and another one shifted to higher temperatures with increased thermal resistance due to stronger interactions with the pore surface. The calorimetric deviation was more significant in Ibu:MCM-41$_{sil}$. This observation seems to contradict what was found for the unloaded matrices, and what was the expected result for surface modification. Nevertheless, ssNMR gave evidence of a higher number of silanol moieties in Ibu:MCM-41$_{sil}$, which was explained as a consequence of the hydrolysis of the methoxy groups presented in the silica surface in acidic conditions offered by the ibuprofen loading; however, in a small extent since the amount of functional organosilane in MCM-41$_{sil}$, was quantified by TGA as 2.03% (w/w).

The TGA analysis also provided the amount of ibuprofen in each composite, 30.88 % in Ibu:MCM-41 and 28.55 % (w/w) in Ibu:MCM-41$_{sil}$, that corresponds to 59.62% and 59.23% (v/v) of pores filling. The amorphization of ibuprofen in the composites was confirmed by the detection of glass transition and the absence of melting in DSC thermograms.

The mathematical model fitting of the release profiles of Ibu:MCM-41 and Ibu:MCM-41$_{sil}$ showed that in both composites the release of ibuprofen is controlled by drug diffusion through the matrices pores. Furthermore, both composites presented nearly an explosive release behavior, evidenced by the initial burst release, although at a slower rate compared with ibuprofen dissolution: maximum of 90% released, comparing with the 100% dissolution of native ibuprofen in the first minute. This slower release rate was more considerable in the Ibu:MCM-41$_{sil}$ evidenced by its smaller rate constant of 1.8789 h^{-1}. Having in mind the ssNMR and DSC results, this was interpreted as due to stronger guest-host interactions that resulted from ibuprofen molecules interacting by hydrogen bonds with a higher amount of silanols, originated from the hydrolysis of the methoxy groups. Therefore, besides successful amorphization, a rational basis to explain the drug release profile was provided.

Moreover, the work allowed the familiarization with different experimental techniques which were not addressed during graduation nor their background as DSC, ssNMR, TGA. Novel theoretical concepts related with condensed matter physics and relaxation phenomena were assimilated, and the ones associated with physical chemistry were more deeply understood. Also, non-conventional and complex data treatment was carried out with non-linear data simulation and spectral deconvolution. Concerning ssNMR, it implied the familiarization wit new software tools

as TopSpin, MestreNova and dmfit. The kinetic modelling of drug release was achieved by using different equations in literature implemented by the student herself.

Finally, the work was accepted to a poster communication in ChemPor 2018.

5 References

1. Stegemann, S., Leveiller, F., Franchi, D., De Jong, H., & Lindén, H. (2007). When poor solubility becomes an issue: from early stage to proof of concept. *European journal of pharmaceutical sciences*, *31*(5), 249-261.

2. Di, L., & Kerns, E. H. (2015). *Drug-like properties: concepts, structure design and methods from ADME to toxicity optimization*. Academic press.

3. Kümmerer K. (2010). Pharmaceuticals in the Environment. *Annual Review of Environment and Resources, 35(1),* 57-75.

4. Rodriguez-Aller, M., Guillarme, D., Veuthey, J. L., & Gurny, R. (2015). Strategies for formulating and delivering poorly water-soluble drugs. *Journal of Drug Delivery Science and Technology*, *30*, 342-351.

5. Kawabata, Y., Wada, K., Nakatani, M., Yamada, S., & Onoue, S. (2011). Formulation design for poorly water-soluble drugs based on biopharmaceutics classification system: basic approaches and practical applications. *International journal of pharmaceutics*, *420*(1), 1-10.

6. Shargel, L., Wu-Pong, S., & Yu, A. B. C. (2012). *Applied Biopharmaceutics & Pharmacokinetics, 6e. New York, NY: McGraw-Hill*.

7. Agee, B. M., Mullins, G., & Swartling, D. J. (2016). Progress towards a more sustainable synthetic pathway to ibuprofen through the use of solar heating. *Sustainable Chemical Processes*, *4*(1), 8.

8. Dudognon, E., Danède, F., Descamps, M., & Correia, N. T. (2008). Evidence for a new crystalline phase of racemic ibuprofen. *Pharmaceutical research*, *25*(12), 2853-2858.

9. Synthesis. www.chm.bris.ac.uk/motm/ibuprofen/synthesis. Accessed February 9, 2018.

10. Reddy, B. B. K., & Karunakar, A. (2011). Biopharmaceutics classification system: a regulatory approach. *Dissolution Technologies*, *18*(1), 31-37.

11. Potthast, H., Dressman, J. B., Junginger, H. E., Midha, K. K., Oeser, H., Shah, V. P., ... & Barends, D. M. (2005). Biowaiver monographs for immediate release solid oral dosage forms: Ibuprofen. *Journal of pharmaceutical sciences*, *94*(10), 2121-2131.

12. IBUPROFEN. www.drugbank.ca/drugs/DB01050. Accessed February 9, 2018.

13. Moura Ramos, J. J., & Diogo, H. P. (2006). Are crystallization and melting the reverse transformation of each other?. *Journal of chemical education*, *83*(9), 1389.

14. Vekilov, P. G. (2010). Nucleation. *Crystal growth & design*, *10*(12), 5007-5019.

15. Debenedetti, P. G., & Stillinger, F. H. (2001). Supercooled liquids and the glass transition. *Nature*, *410*(6825), 259.

16. Richert, R. (2015). Probing liquid dynamics, one molecule at a time. *Proceedings of the National Academy of Sciences*, *112*(16), 4841-4842.

17. ALOthman, Z. (2012). A review: fundamental aspects of silicate mesoporous materials. *Materials*, *5*(12), 2874-2902.

18. Grün, M., Unger, K. K., Matsumoto, A., & Tsutsumi, K. (1999). Novel pathways for the preparation of mesoporous MCM-41 materials: control of porosity and morphology. *Microporous and mesoporous materials*, *27*(2-3), 207-216.

19. Manzano, M., Aina, V., Arean, C. O., Balas, F., Cauda, V., Colilla, M., ... & Vallet-Regi, M. (2008). Studies on MCM-41 mesoporous silica for drug delivery: effect of particle morphology and amine functionalization. *Chemical Engineering Journal*, *137*(1), 30-37.

20. Song, S. W., Hidajat, K., & Kawi, S. (2005). Functionalized SBA-15 materials as carriers for controlled drug delivery: Influence of surface properties on matrix− drug interactions. *Langmuir*, *21*(21), 9568-9575.

21. Ye, W., Lin, Z., Dong, B., Kang, J., Zheng, X., & Wang, X. (2011). Preparation and catalytic properties of Ti-SBA-15 mesoporous materials. *Materials Sciences and Applications*, *2*(06), 661.

22. Akinjokun, A. I., Ojumu, T. V., & Ogunfowokan, A. O. (2016). Biomass, Abundant Resources for Synthesis of Mesoporous Silica Material. In *Microporous and Mesoporous Materials*. InTech.

23. Der Voort, P. V., & Vansant, E. F. (1996). Silylation of the silica surface a review. *Journal of liquid chromatography & related technologies*, *19*(17-18), 2723-2752.

24. Cerveny, S., Schwartz, G. A., Otegui, J., Colmenero, J., Loichen, J., & Westermann, S. (2012). Dielectric study of hydration water in silica nanoparticles. *The Journal of Physical Chemistry C*, *116*(45), 24340-24349.

25. Fryxell, G. E. (2006). The synthesis of functional mesoporous materials. *Inorganic Chemistry Communications*, *9*(11), 1141-1150.

26. Iliade, P., Miletto, I., Coluccia, S., & Berlier, G. (2012). Functionalization of mesoporous MCM-41 with aminopropyl groups by co-condensation and grafting: a physico-chemical characterization. *Research on Chemical Intermediates*, *38*(3-5), 785-794.

27. Silverstein, R. M., Webster, F. X., Kiemle, D. J., & Bryce, D. L. (2014). *Spectrometric identification of organic compounds*. John wiley & sons.

28. Elmer, P. (2005). FT-IR Spectroscopy Attenuated Total Reflectance (ATR). *Technical Note*, *27*(11).

29. Zhang P. Adsorption and Desorption Isotherms. http://www.keresearchgroup.com/uploads/4/8/4/5/48456521/160903_introduction_to_bet

_isotherms.pdf. Published 2016. Accessed July 11, 2018.

30. Sing, K. S. (1985). Reporting physisorption data for gas/solid systems with special reference to the determination of surface area and porosity (Recommendations 1984). *Pure and applied chemistry*, *57*(4), 603-619.

31. Schurko R. Introduction to Solid State NMR. http://mutuslab.cs.uwindsor.ca/schurko/ssnmr/ssnmr_schurko.pdf. Accessed July 11, 2018.

32. Zhao, X. S., Lu, G. Q., Whittaker, A. K., Millar, G. J., & Zhu, H. Y. (1997). Comprehensive study of surface chemistry of MCM-41 using 29Si CP/MAS NMR, FTIR, pyridine-TPD, and TGA. *The Journal of Physical Chemistry B*, *101*(33), 6525-6531.

33. Dirè, S., Pagani, E., Babonneau, F., Ceccato, R., & Carturan, G. (1997). Unsupported SiO 2-based organic–inorganic membranes. *Journal of Materials Chemistry*, *7*(1), 67-73.

34. Yasmin, T., & Müller, K. (2016). Structural characterization of octadecyl modified MCM-41 silica by NMR and FTIR. *Journal of Porous Materials*, *23*(2), 339-348.

35. Azaïs, T., Tourné-Péteilh, C., Aussenac, F., Baccile, N., Coelho, C., Devoisselle, J. M., & Babonneau, F. (2006). Solid-state NMR study of ibuprofen confined in MCM-41 material. *Chemistry of Materials*, *18*(26), 6382-6390.

36. Soares, C. M., dos Santos, O. A., de Castro, H. F., Itako, J. E., de Moraes, F. F., & Zanin, G. M. (2006). NMR characterization of the role of silane precursors on the catalytic activity of sol–gel encapsulated lipase. *Journal of non-crystalline solids*, *352*(32-35), 3469-3477.

37. PerkinElmer.Thermogravimetric Analysis (TGA) A Beginner's Guide. https://www.perkinelmer.com/CMSResources/Images/4474556GDE_TGABeginnersGuide.pdf. Accessed July 11, 2018.

38. Gotro J. Thermoset Characterization Part 12: Introduction to Thermogravimetric Analysis (TGA). https://polymerinnovationblog.com/thermoset-characterization-part-12-introduction-thermogravimetric-analysis-tga/. Published 2014. Accessed July 11, 2018.

39. Clas, S. D., Dalton, C. R., & Hancock, B. C. (1999). Differential scanning calorimetry: applications in drug development. *Pharmaceutical science & technology today*, *2*(8), 311-320.

40. Lukas, K., & LeMaire, P. K. (2009). Differential scanning calorimetry: fundamental overview. *Resonance*, *14*(8), 807-817.

41. Gao, L., Wang, Y., Wang, J., Huang, L., Shi, L., Fan, X., ... & Li, Z. (2006). A novel ZnII-sensitive fluorescent chemosensor assembled within aminopropyl-functionalized mesoporous SBA-15. *Inorganic chemistry*, *45*(17), 6844-6850.

42. Barrera, E. G., Livotto, P. R., & dos Santos, J. H. (2016). Hybrid silica bearing different

organosilanes produced by the modified Stöber method. *Powder Technology*, *301*, 486-492.

43. Wu, S., Wang, J., Liu, G., Yang, Y., & Lu, J. (2012). Separation of ethyl acetate (EA)/water by tubular silylated MCM-48 membranes grafted with different alkyl chains. *Journal of membrane science*, *390*, 175-181.

44. Lestari, W. W., Arvinawati, M., Martien, R., & Kusumaningsih, T. (2018). Green and facile synthesis of MOF and nano MOF containing zinc (II) and benzen 1, 3, 5-tri carboxylate and its study in ibuprofen slow-release. *Materials Chemistry and Physics*, *204*, 141-146.

45. J Jin, X., Wang, Q., Sun, J., Panezai, H., Bai, S., & Wu, X. (2017). Dual (pH-and temperature-) stimuli responsive nanocarrier with bimodal mesoporous silica nanoparticles core and copolymer shell for controlled ibuprofen-releasing: Fractal feature and diffusion mechanism. *Microporous and Mesoporous Materials*, *254*, 77-85.

46. Dabiri, S. M. H., Lagazzo, A., Barberis, F., Shayganpour, A., Finocchio, E., & Pastorino, L. (2017). New in-situ synthetized hydrogel composite based on alginate and brushite as a potential pH sensitive drug delivery system. *Carbohydrate polymers*, *177*, 324-333.

47. Adeoye, O., Costa, C., Casimiro, T., Aguiar-Ricardo, A., & Cabral-Marques, H. (2018). Preparation of ibuprofen/hydroxypropyl-γ-cyclodextrin inclusion complexes using supercritical CO2-assisted spray drying. *The Journal of Supercritical Fluids*, *133*, 479-485.

48. Ziaee, A., Albadarin, A. B., Padrela, L., Faucher, A., O'reilly, E., & Walker, G. (2017). Spray drying ternary amorphous solid dispersions of ibuprofen–An investigation into critical formulation and processing parameters. *European Journal of Pharmaceutics and Biopharmaceutics*, *120*, 43-51.

49. Daneluti, A. L. M., Neto, F. M., Velasco, M. V. R., Baby, A. R., & do Rosário Matos, J. (2018). Evaluation and characterization of the encapsulation/entrapping process of octyl methoxycinnamate in ordered mesoporous silica type SBA-15. *Journal of Thermal Analysis and Calorimetry*, *131*(1), 789-798.

50. Salam, M. S. A., Betiha, M. A., Shaban, S. A., Elsabagh, A. M., & El-Aal, R. M. A. (2015). Synthesis and characterization of MCM-41-supported nano zirconia catalysts. *Egyptian Journal of Petroleum*, *24*(1), 49-57.

51. Webb, L. J., Rivillon, S., Michalak, D. J., Chabal, Y. J., & Lewis, N. S. (2006). Transmission infrared spectroscopy of methyl-and ethyl-terminated silicon (111) surfaces. *The Journal of Physical Chemistry B*, *110*(14), 7349-7356.

52. Costa, J. A. S., de Jesus, R. A., da Silva, C. M. P., & Romão, L. P. C. (2017). Efficient adsorption of a mixture of polycyclic aromatic hydrocarbons (PAHs) by Si–MCM–41 mesoporous molecular sieve. *Powder Technology*, *308*, 434-441.

53. Léon, C. I. S., Song, D., Su, F., An, S., Liu, H., Gao, J., ... & Leng, J. (2015). Propylsulfonic

acid and methyl bifunctionalized TiSBA-15 silica as an efficient heterogeneous acid catalyst for esterification and transesterification. *Microporous and Mesoporous Materials*, *204*, 218-225.

54. Wencel, D., Barczak, M., Borowski, P., & McDonagh, C. (2012). The development and characterisation of novel hybrid sol–gel-derived films for optical pH sensing. *Journal of Materials Chemistry*, *22*(23), 11720-11729.

55. Yoshikawa, M., Shiba, H., Kanezashi, M., Wada, H., Shimojima, A., Tsuru, T., & Kuroda, K. (2017). Synthesis of a 12-membered cyclic siloxane possessing alkoxysilyl groups as a nanobuilding block and its use for preparation of gas permeable membranes. *RSC Advances*, *7*(77), 48683-48691.

56. Brás, A. R., Noronha, J. P., Antunes, A. M., Cardoso, M. M., Schönhals, A., Affouard, F., ... & Correia, N. T. (2008). Molecular motions in amorphous ibuprofen as studied by broadband dielectric spectroscopy. *The Journal of Physical Chemistry B*, *112*(35), 11087-11099.

57. Barnabas, M. J., Parambadath, S., & Ha, C. S. (2017). Amino modified core–shell mesoporous silica based layered double hydroxide (MS-LDH) for drug delivery. *Journal of industrial and engineering chemistry*, *53*, 392-403.

58. Brás, A. R., Fonseca, I. M., Dionísio, M., Schönhals, A., Affouard, F., & Correia, N. T. (2014). Influence of nanoscale confinement on the molecular mobility of ibuprofen. *The Journal of Physical Chemistry C*, *118*(25), 13857-13868.

59. Cordeiro, T., Santos, A. F., Nunes, G., Cunha, G., Sotomayor, J. C., Fonseca, I. M., ... & Viciosa, M. T. (2016). Accessing the physical state and molecular mobility of naproxen confined to nanoporous silica matrixes. *The Journal of Physical Chemistry C*, *120*(26), 14390-14401.

60. National Institute of Standarts and Technology. Ibuprofen. Livro de Química na Web. https://webbook.nist.gov/cgi/cbook.cgi?ID=C15687271&Mask=4#. Published 2017. Accessed July 26, 2018.

61. Salmerón Sánchez, M., Mathot, V. B., Vanden Poel, G., & Gómez Ribelles, J. L. (2007). Effect of the cooling rate on the nucleation kinetics of poly (L-lactic acid) and its influence on morphology. *Macromolecules*, *40*(22), 7989-7997.

62. Brás, A. R., Merino, E. G., Neves, P. D., Fonseca, I. M., Dionísio, M., Schönhals, A., & Correia, N. T. (2011). Amorphous ibuprofen confined in nanostructured silica materials: a dynamical approach. *The Journal of Physical Chemistry C*, *115*(11), 4616-4623.

63. Mello, V. A. D., & Ricci-Júnior, E. (2011). Encapsulation of naproxen in nanostructured system: structural characterization and in vitro release studies. *Quimica Nova*, *34*(6), 933-939.